ACS OMEGA

Open Access



http://pubs.acs.org/journal/acsodf

Article

# In Vitro Targeted Delivery of Simvastatin and Niacin to Macrophages Using Mannan-Grafted Magnetite Nanoparticles

Banafsheh Rastegari, Atefe Ghamar Talepoor, Shahdad Khosropanah, and Mehrnoosh Doroudchi*

Cite This: *ACS Omega* 2024, 9, 658−674

Read Online

ACCESS | Metrics & More | Article Recommendations | Supporting Information

**ABSTRACT:** Atherosclerosis, a leading cause of mortality worldwide, involves various subsets of macrophages that contribute to its initiation and progression. Current treatment approaches focus on systemic, long-term administration of cholesterol-lowering antioxidants such as statins and certain vitamins, which unfortunately come with prolonged side effects. To overcome these drawbacks, a mannose-containing magnetic nanoparticle (NP) is introduced as a drug delivery system to specifically target macrophages in vitro using simvastatin or niacin and a combinational therapy approach that reduces local inflammation while avoiding unwanted side effects. The synthesized NPs exhibited superparamagnetic behavior, neutrally charged thin coating with a hydrodynamic size of 77.23 ± 13.90 nm, and a metallic core ranging from 15 to 25 nm. Efficient loading of niacin (87.21%) and simvastatin (75.36%) on the NPs was achieved at respective weights of 20.13 and 5.03 (w/w). In the presence of a mannan hydrolyzing enzyme, 79.51% of simvastatin and 67.23% of niacin were released from the NPs within 90 min, with a leakage rate below 19.22%. Additionally, the coated NPs showed no destructive effect on J774A macrophages up to a concentration of 200 $\mu$g/mL. Simvastatin-loaded NPs exhibited a minimal increase in *IL-6* expression. The low dosage of simvastatin decreased both *IL-6* and *ARG1* expressions, while niacin and combined simvastatin/niacin increased the level of *ARG1* expression significantly. Toxicity evaluations on human umbilical vein endothelial cells and murine liver cells revealed that free simvastatin administration caused significant toxicity, whereas the encapsulated forms of simvastatin, niacin, and a combination of simvastatin/niacin at equivalent concentrations exhibited no significant toxicity. Hence, the controlled release of the encapsulated form of simvastatin and niacin resulted in the effective modulation of macrophage polarization. The delivery system showed suitability for targeting macrophages to atherosclerotic plaque.

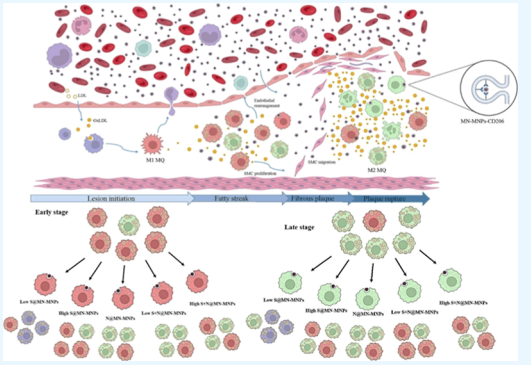


## 1. INTRODUCTION

Atherosclerosis is one of the leading causes of coronary artery disease, which is considered as one of the most societal healthcare challenges in recent decades.[1] Atherosclerosis is a chronic inflammatory process in which immune cells react with metabolic risk factors, resulting in initiating, spreading, and activating lesions in large- and medium-sized arteries. Clot formation by the atherosclerotic plaque causes tissue infarction, unstable angina, and many sudden deaths, all of which are termed acute coronary syndromes. Macrophages play a very special role in the development and progression of atherosclerosis. Activation of atherosclerosis-associated macrophages (AAM) causes endothelial disruption, rupture of blood vessels, and subsequently infarction.[2] Accordingly, many treatments have been identified and introduced to reduce the complications of atherosclerosis and delay or prevent infarction. Prevention and treatment of atherosclerosis is mainly focused on reducing the burden of atherosclerotic plaques and the stability of vulnerable plaques by inhibiting activated cells such as macrophages and T lymphocytes, inhibiting smooth muscle cell proliferation and platelet formation.[3−5] Therapeutic approaches can be divided into four categories, which include anti-inflammatory, antithrombotic, antiproliferative, and immunosuppressive drugs. The statin family with anti-inflammatory and cholesterol-lowering activity,[6] sirolimus/rapamycin with immunosuppressant property and inhibition of smooth muscle cell migration, paclitaxel, and actinomycin D with inhibitory effects on smooth muscle cell migration and proliferation, zetarolimus and orolimus with inhibitory effects on smooth muscle cell proliferation and T lymphocytes, tacrolimus with suppressive effects on the immune system, and dexamethasone with anti-inflammatory properties are the most used medicines for atherosclerosis.[7]

Among the common drugs that are prescribed for patients with atherosclerosis, statins and niacin can be named. In addition to regulating cholesterol synthesis, statins also have

Received: August 27, 2023
Revised: November 25, 2023
Accepted: November 29, 2023
Published: December 18, 2023

beneficial effects on cardiovascular disease through regulating anti-inflammatory/pro-inflammatory responses. Interestingly, statin-mediated inhibition of the mevalonate pathway exerts specific induction of IL-1 family pro-inflammatory cytokines through direct maturation (IL-1$\beta$ and IL-18) and indirect (IL-1$\alpha$) using caspase-1.[8−10] On the other hand, simvastatin, atorvastatin, fluvastatin, and pravastatin have been shown to reduce *IL-6* production by 53, 50, 64, and 60% of coculture of vascular smooth muscle cells with mononuclear human cells, respectively. While these findings pointed to the anti-inflammatory effect of statin drugs on macrophages, they also linked statins to inflammasome formation and diabetes.[11,12] It is shown that simvastatin increases ox-LDL-induced macrophage autophagy and reduces fat accumulation which could be a potential target of simvastatin in plaque stabilization.[13] In general, statins reduce plaque size through decreasing the macrophage population by preventing intima penetration by monocytes in human and mouse models. Hence, macrophage accumulation in atherosclerotic plaques decreases. However, reduced proliferation and thus reduced macrophage population are observed only in response to a decrease in serum LDL cholesterol and lipid content in rat and human aortic carotid artery plaques. These results suggest that macrophage proliferation as a determinant of atherosclerosis progression and is an attractive target for plaque regression in the prevention and treatment of atherosclerosis.[14]

Niacin plays a role in creating and enhancing anti-inflammatory immune responses in humans and animal models.[15] The beneficial effects of niacin on plasma lipids and lipoproteins were first described in the 1950s.[16] According to a meta-analysis of 30 randomized controlled trials, niacin potentially reduced 15−30% of triglycerides (TG) and increased 10−25% of HDL (HDL-C) cholesterol, while it only slightly decreased total plasma cholesterol (TC). These results indicated that niacin has a protective effect against the progression of atherosclerosis.[17]

Niacin was later found to work mainly by lowering non-HDL cholesterol and moderately increasing HDL, resulting in greater anti-inflammatory effects and, subsequently, prevention of atherosclerotic plaque development, which may be of clinical importance. Having said so, both statins and niacin treatment regiments include systemic long-term treatment and have side effects such as muscle breakdown, liver problems, stomach ulcers, myopathy, as well as blood sugar elevation and diabetes.[18] Therefore, selective targeting of plaque macrophages may provide a means to reduce local inflammation and avoid unwanted side effects of therapy. In recent years, several advantages such as cost-effectiveness, optimized bioavailability, drug concentration balance, reduced side effects with controlled release, and improved stability and solubility of hydrophobic drugs have led many scientists to the use of drug delivery systems. Despite intensive efforts in the targeted treatment of cardiovascular diseases with the help of drug delivery nanosystems, only a few positive outcomes have been achieved.[19,20] Magnetic nanoparticles (NPs) are considered as one of the attractive nanostructures in clinical applications due to their bifunctional ability in diagnosis (contrast agent) and drug delivery systems.[21,22] Moreover, the "magnetic drug delivery" helps out the effective elevation of drug payloads in the target site, at the same time diminishing their systemic toxicity in thrombosis, cardiac ischemia, and several cancer models.[23−25]

Specific targeting of macrophages can be optimized using cellular receptors, among which lectin receptors can be named. Lectin receptors function in energy supply, innate immune system identification, endocytosis, and many other activities.[26] Several lectin receptors have been proposed for the diagnosis and treatment of various diseases such as cancer and atherosclerosis, including complement receptor 3, galactose, and mannose receptors. So far, several mannose-binding lectins like (CD206 and CD280/MRC2) Collagen Endo180 have been proposed in connection with the diagnosis and treatment of a variety of diseases.[27−29] Due to the presence of cytokines such as IL-4, the activated state of macrophages, and the high expression of mannose receptors in the atherosclerotic plaque region,[30] these receptors can be promising in the specific targeting of activated macrophages in atherosclerotic arteries.

Until now, several subsets of macrophages are discovered, of which the two main subsets are M1 and M2.[31] Both subsets of macrophages are known to play a role in different stages of the development of atherosclerosis plaque.[32] Accordingly, the M2 subset of macrophages has a protective role against the atherosclerosis progression, while M1 macrophages have a critical role in the enlargement and progression of atherosclerotic lesions.[5,33] Therefore, one may expect that shifting M1 to M2 macrophages would be one of the hallmarks of plaque stabilization and prevent progression of the diseases.[34]

Targeted delivery to macrophages have been focused on the CD40 molecule which has diverse stimulatory function.[35] First attempt was reported using a pH-sensitive polymer micelle-targeted mannose receptor (CD206) for siRNA transfer.[36] Also, some glycosylated micelles have been used to block macrophage receptors MSR1 and CD36 and hence reduce oxLDL uptake and accumulation.[37,38] A delivery system of polyethylene (amidoamine) dendrimer (PAMAM) with PEG-coated anhydride has been designed for targeting folic acid receptor-expressing macrophages in vitro.[39] A dextran sulfate-coated HDL delivery system was used to transport atorvastatin to atherosclerotic associated macrophages due to the high affinity to scavenger receptor class AI (SR-AI), to reduce ox-LDL uptake, and induce cholesterol efflux.[40] A new CD44-targeted hyaluronan (HA) nanostructure containing atorvastatin was shown significant anti-inflammatory effects on macrophages compared with free atorvastatin in vitro and also decrease inflammation of apolipoprotein (ApoE) E-deficient mouse model harboring advanced plaque using magnetic resonance imaging.[41] Herein, due to the limited studies on the targeted carriers with the ability of codelivery of common medications to inflammatory cells, we studied mannan NPs loaded with simvastatin and/or niacin, which are currently in use as free drugs, to evaluate specific targeting of macrophages and the potential of future use of the simvastatin/niacin-loaded magnetic NPs (simvastatin/niacin-loaded MN-MNPs) in atherosclerotic plaque macrophages.

## 2. MATERIALS AND METHODS

**2.1. Materials.** Iron(III) chloride hexahydrate, iron(II) chloride tetrahydrate, and liquid ammonia (analytical grade) were purchased from Merck (Merck Inc., NJ, USA). Locust bean gum from *Ceratonia siliqua* seeds, niacin, simvastatin, and MTT ([3−4, 5-dimethylthiazol-2-yl]-2, 5-diphenyltetrazolium bromide) were purchased from Sigma-Aldrich (St. Louis, MO, USA) without further treatments. Dulbecco's modified Eagle's


https://doi.org/10.1021/acsomega.3c06389
ACS Omega 2024, 9, 658−674

medium (DMEM), DMEM/HamsF12, trypsin, penicillin/streptomycin, and fetal bovine serum (FBS) were obtained from Gibco (Gaithersburg, USA). The J774A cell line and human umbilical vein endothelial cell (HUVEC) line were obtained from the Pasteur Institute of Iran (Tehran, Iran).

**2.2. MN-MNP Synthesis and Characterization.** One-spot synthesis of mannan-coated magnetic NPs (MN-MNPs) was performed according to the former procedure with some modifications.[42] The initial mixture was composed of 100 mL of distilled water containing 2.0 g of $FeCl_2{\cdot}4H_2O$ and 5.2 g of $FeCl_3{\cdot}6H_2O$, with 1200 rpm stirring, at 90 °C under $N_2$ protection. After adding 50 mL of mannan solution (2.0 g/L), ammonium hydroxide (30%) was added dropwise within 15 min to crystallize the magnetic NPs until the pH reached up to 10.0. In the following procedure, the mixture was incubated at the same temperature for an additional 45 min, followed by cooling with ice-cold water. Finally, the MN-MNPs were separated from the solution with the help of the 0.6 T permanent external magnet, rinsed with 50 mL of water three times, and dried in a vacuum oven at 70 °C.

The crystalline properties and phase identification were recorded on an X-ray diffractometer (Bruker, D8ADVANCE, Germany). The diffractogram was obtained by using Cu−K$\alpha$ radiation in the range $10° < 2\theta° < 90°$. The magnetic behavior was investigated on random assembly of particles at room temperature with a maximum applied field of 10 kOe and a sensitivity of $10^{-3}$ emu by a vibrating sample magnetometer (VSM, Dexing, Model: 250). Mannan grafting was approved by a Fourier transform infrared (FT-IR) spectrometer (Thermo Fisher Scientific Inc.) in a frequency interval of 4000−400 $cm^{-1}$. The morphology and size of dried NPs were observed by Transmission Electron Microscopy (JEOL-JEM 1200EX, Japan) operated with an 80 kV microscope. For this purpose, 500 $\mu$L of sample dispersion with a concentration of 1 mg/mL was prepared; then, a drop of it was fixed onto carbon support on copper grids (200 meshes), and the grid surface was air-dried at room temperature for TEM imaging. The mean hydrodynamic size and polydispersity index were characterized through dynamic light scattering (DLS) experiments using 0.1% w/v ethylene glycol NP dispersions (HORIBA SZ-100, Japan). The $\zeta$ potentials of the synthesized NPs were also measured in PBS buffer by using a HORIBA SZ-100.

**2.3. Drug Loading and Release.** The simvastatin and niacin stock solutions were prepared in methanol and PBS with final concentrations of 5 and 20 mg/mL, respectively. To prepare simvastatin, niacin, and simvastatin/niacin-loaded magnetic NPs through the adsorption process, 10 mg of MN-MNPs was dispersed for 10 min. Then, 5 mL of niacin (1 mg/mL, PBS buffer solution, pH ∼ 7.4) was added to NPs and rotated for 16 h at 4 °C. On the next day, the NPs were then washed twice with PBS, and simvastatin was added sequentially to the PBS solution with a final concentration of 50 $\mu$g/mL at the same above condition. Finally, the unbound niacin and simvastatin were calculated using a standard curve obtained from high-performance liquid chromatography (HPLC). The drug loading was calculated as follows

$$\%\text{Drug loading content} = \frac{\text{Cl}\cdot\text{Vl}}{\text{MNPs}} \times 100 \quad (1)$$

In this equation, Cl and Vl are defined as loaded drug concentration and volume, while MNPs come from the mass of MN-MNPs.

The encapsulation efficiency of MN-MNPs is as follows. The Drug@MN-MNPs were collected with an external magnet, and then 10 mL of methanol solutions was added to the mixture with a vortex for 10 min to completely dissolve entrapped simvastatin, niacin, or both. The drug content was determined by monitoring the concentration through a $\lambda_{max}$ of 273 nm. The drug encapsulation efficiency is calculated as follows

$$\text{Encapsulation efficiency (\%)} = (\text{drug initial weight (mg)} - \text{unloaded drug in the aqueous phase (mg)})/(\text{drug initial weight (mg)}) \times 100 \quad (2)$$

The in vitro release study of MN-MNPs, simva@MN-MNPs (S@MN-MNPs), niacin@MN-MNPs (N@MN-MNPs), and simvastatin/niacin@MN-MNPs (S + N@MN-MNPs) was carried out at 37 °C under 30 rpm rotating conditions in the dark. Initially, 10 mg of drug-loaded MNPs (containing 2 mg niacin and 0.5 mg simvastatin) was dispersed in 10 mL of PBS, pH ∼ 8.0 containing 1 mg/mL BSA as the most abundant protein in the bloodstream. Then, 0.02 U of mannanase was added separately to the solution. After the appropriate time, NPs were collected by an external magnet, and 500 $\mu$L aqueous solutions were collected. The released drug was finally calculated using UV-HPLC, a previously used method, with small modifications.[43] The simvastatin and niacin standard solutions were prepared by dissolving them in absolute ethanol and water in final concentrations of 10 mg/mL. The serial dilution was further done by dissolving drugs in HPLC grade water at the range of 6.25−250 $\mu$g/mL for simvastatin and niacin 12.5−800 $\mu$g/mL. The C18 column was applied for detection of aqueous solution containing simvastatin/niacin. 30 $\mu$L of each sample was injected onto a pre-equilibrated column with a mobile phase consisting of methanol:water (80:20, v/v, AZURA column, 150 × 4.6 mm, Germany) at a flow rate of 1 mL/min for 10 min. The UV detector was set at a wavelength of 237 nm for both simvastatin and niacin.

**2.4. Cell Isolation and Culture.** Murine macrophage cell line, J774A, and HUVECs were grown in Dulbecco's modified Eagle's medium (DMEM) and DMEM/HamsF12 medium containing 10% FBS and 1% penicillin/streptomycin, respectively. As described by Shen et al. and Charni-Natan et al.[44,45] for isolation of hepatic cells, mice of 10 weeks of age were anesthetized with 100 $\mu$L of ketamine (120 mg/kg) and xylazine (18 mg/kg). Then, the perfusion was started from hepatic vena cava with a peristaltic pump (a flow rate of 5 mL/min) for 15 min with perfusion solution (Hank's buffer containing EDTA 0.5 mM without calcium and magnesium). After infiltration of blood, digestion buffer (Hank's buffer with calcium and magnesium and 1 mg/mL collagenase I and IV) was added with a slower flow rate (3 mL/min) for 30 min. After that, the hepatic tissue was transferred to a sterile plate and cut into smaller pieces to isolate the primary cells. The supernatant containing cells were centrifuged at 200$g$ for 10 min at 4 °C. Finally, mice hepatic cells were cultured in low-glucose DMEM for further analysis.

Cell toxicity was determined with the help of the MTT assay. For this purpose, a total number of $1.5 \times 10^4$, $3.0 \times 10^4$, and $3.0 \times 10^4$ of HUVECs, J774A, and normal murine hepatocyte cells were seeded into 96-well cell culture plates in the above-mentioned culture conditions overnight at 37.0 °C


https://doi.org/10.1021/acsomega.3c06389
ACS Omega 2024, 9, 658−674

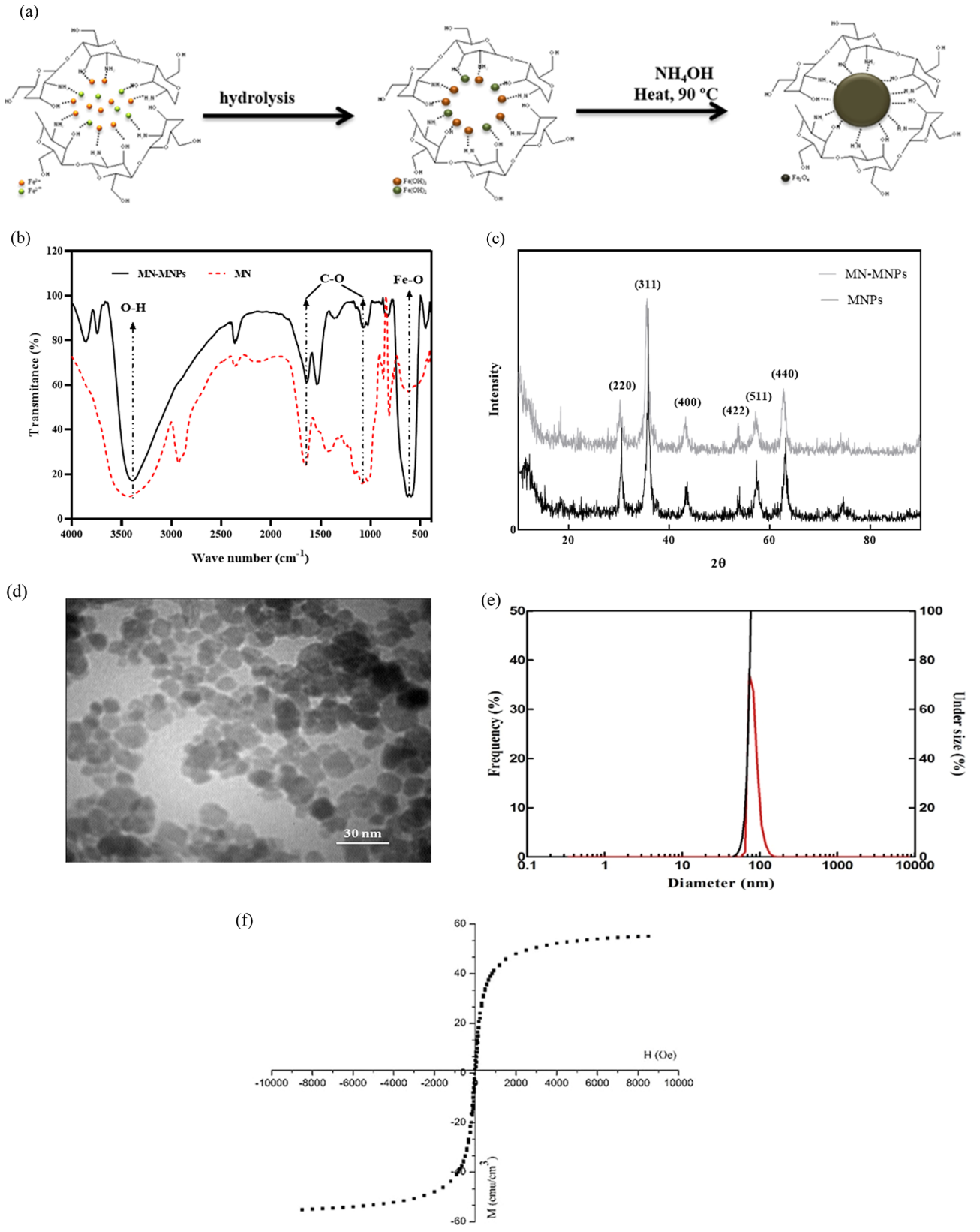


**Figure 1.** (a) Synthesis and physicochemical characteristic procedure of MN-MNPs. (b) IR spectrum and (c) XRD diagram of MN and MN-MNPs. (d) TEM image and (e) hydrodynamic size of MN-MNPs using dynamic light scattering. (f) Magnetic behavior of the MN-MNPs.

under a humidified atmosphere of 5% $CO_2$. The cytotoxicity of simvastatin, niacin, MN-MNPs, S@MN-MNPs, N@MN-MNPs, and S + N@MN-MNPs was investigated at different concentrations for 24 and 48 h. Then, cells were washed twice with PBS and incubated in a fresh medium containing 10 $\mu$L of the MTT solution (5.0 mg/mL of cell culture medium), and plates were wrapped with aluminum foil for further incubation at 37.0° for 4 h C. After that, the culture medium



https://doi.org/10.1021/acsomega.3c06389
ACS Omega 2024, 9, 658−674

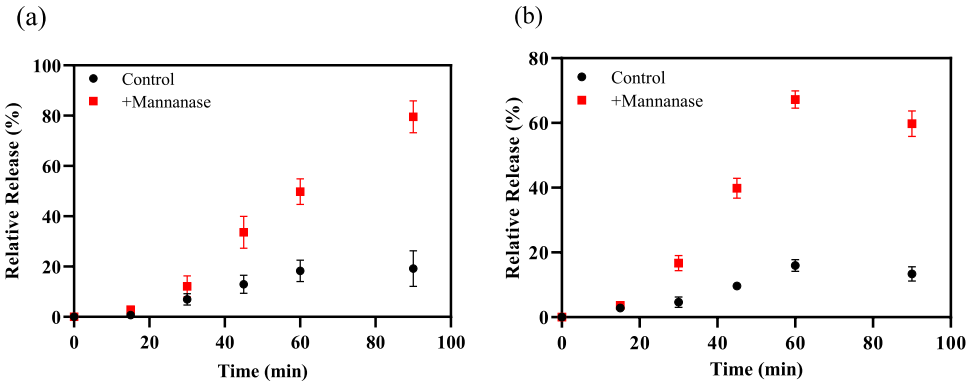


**Figure 2.** Release profile of (a) simvastatin and (b) niacin upon treatment of 0.02 U of mannanase onto the niacin@MN-MNPs in the presence and absence of the mannanase degrading enzyme. The experiment was repeated three times and represented as mean ± STDEV. The PBS solution, pH 7.4, was chosen as an untreated control condition.

was removed, and the formazan crystals were dissolved in 100% DMSO. The absorbance was measured at 570 nm using a Tecan infinite-200 M Pro colorimeter (Tecan Co., Switzerland). The surviving percentage was calculated using the following formula

$$\text{Viability (\%)} = \frac{\text{sample absorbance}}{\text{negative control absorbance}} \times 100 \quad (3)$$

**2.5. Macrophage Stimulation, RNA Extraction, and Real-Time PCR Analysis.** Macrophages were treated, for 24 and 48 h, with LPS (100 ng/mL, Sigma-Aldrich, St. Louis, Missouri, USA) and IFN-$\gamma$ (50 $\mu$g/mL, Biolegend) to generate the M1 subset and IL-4 (75 $\mu$g/mL, Biolegend, San Diego, California, USA) to generate the M2 subset. Macrophages were seeded in six-well plates, allowed to adhere overnight, and treated with indicated concentrations of LPS/IFN-$\gamma$ and IL-4, and then expression levels of *IL-6* and *ARG-1* were monitored in the following procedure. After optimizing the M1/M2 treatment conditions, the cells were also treated with different concentrations of simvastatin, niacin, simvastatin/niacin, and also MN-MNPs, S@MN-MNPs, N@MN-MNPs, and S + N@MN-MNPs for 24 and 48 h. Then, total RNA extractions were performed (RNA extraction kit, Parstus Co., Iran) from 2 × $10^6$ of J774A cells that were treated with simvastatin, niacin, simvastatin/niacin, and also MN-MNPs, S@MN-MNPs, N@MN-MNPs, and S + N@MN-MNPs at 24 and 48 h time points. Afterward, the reverse transcription procedure was done using an RT reagent kit and oligo-dT primers by the provider's instructions (SMOBio Inc., Taiwan). The sequences of primers are as follows: *ARG1* (F. primer: 5′-AAGACAGGGCTCCTTTCAGG-3′ and R. primer: 5′-AGCAAGCCAAGGTTAAAGCC-′); *IL-6* (F. primer: 5′-TCTGCAAGAGACTTCCATCCA-3′ and R. primer: AGA-CAGGTCTGTTGGGAGTG-3′); and $\beta$-actin (F. primer: 5′-CCAGGGTGTGATGGTGGGAATG-3′ and R. primer: 5′-TGTAGAAGGTGTGGTGCCAGATC-3′). Real-time PCR was performed with the help of the SYBR Green master mix (Amplicon, lnc, Denmark). The reaction mixture contained 1.5 $\mu$L of cDNA, 4 pmol of forward and reverse primers, and 12.5 $\mu$L of SYBR Premix, in RNase-free $H_2O$. The thermal cycling process was then accomplished using the Applied Biosystems (ABI) Step One Plus (Applied Biosystems Step One, USA). The cycling program is set as follows: initial denaturation at 95 °C for 5 min, followed by 40 cycles of denaturation at 95 °C for 30 s, annealing at 60 °C for 30 s, and extension at 72 °C for 45 s. At the end of each reaction, the melting curve analysis from 60 to 95 °C in 0.3 °C increments at 5 s/step was carried out. The comparative Ct method ($2^{\Delta\Delta Ct}$ method) was applied to acquire the range of *IL-6* and *ARG-1* mRNA levels normalized to that of the *β-Actin* housekeeping gene, and the relative expression of mRNA was evaluated.

**2.6. Flow Cytometry.** To investigate the apoptosis/necrosis induced by simvastatin, niacin, simvastatin/niacin, and also MN-MNPs, S@MN-MNPs, N@MN-MNPs, and S + N@MN-MNPs, cells were stained with Annexin-V-PE and 7-AAD after treatment according to the manufacturer's procedure (Biolegend Ltd., USA). Then, the cells were analyzed on a BD FACS Calibur Flow Cytometer (BD Bioscience Ltd., USA), with postprocessing in FlowJo (Tree Star Inc., USA). For each condition, 10,000 events were enumerated and gated on forward and side scatters to select intact single cells.

**2.7. Statistical Analysis.** The results from triplicate MTT and real-Time PCR experiments were averaged and statistically analyzed using mean ± standard deviation, nonparametric *t*-test (Mann−Whitney), nonparametric one-way ANOVA (Kruskal−Wallis), and a p-value less than 0.05 was considered statistically significant.

## 3. RESULTS

**3.1. NP Characterization.** MN-MNPs were synthesized using a one-pot synthesis procedure via in situ coprecipitation of $Fe^{3+}/Fe^{2+}$ ions in the presence of ammonium solutions and mannan as the capping polymer. In this manner, a collection of magnetite NPs entrapped in the mannan polymer were generated (Figure 1a). The presence of polysaccharides within the synthesized NPs was characterized by FT-IR spectroscopy. The FT-IR spectra of mannan polymer (MN) and mannan polymer-coated MNP (MN-MNPs) are shown in 400−4000 $cm^{-1}$ wavenumber (see Figure 1b). Accordingly, the unique peak in the MN-MNP sample at 586 $cm^{-1}$ shows the tetrahedral sites of the Fe−O bonds. The broad band at 3300−3500 $cm^{-1}$ is related to −OH stretching vibration of both mannan polymer and MNPs. The mannan capping polymer is characterized through a 945 $cm^{-1}$ peak (antisymmetric glycoside $\upsilon$a (C−O−C)) and 1029, 1157, and 1654 $cm^{-1}$ peaks (coupled $\upsilon$ (C−C/C−O) stretch vibration), which obviously can be seen in both MN and MN-MNP samples.[46] Moreover, two peaks in 2922 and 2861 $cm^{-1}$


https://doi.org/10.1021/acsomega.3c06389
ACS Omega 2024, 9, 658−674

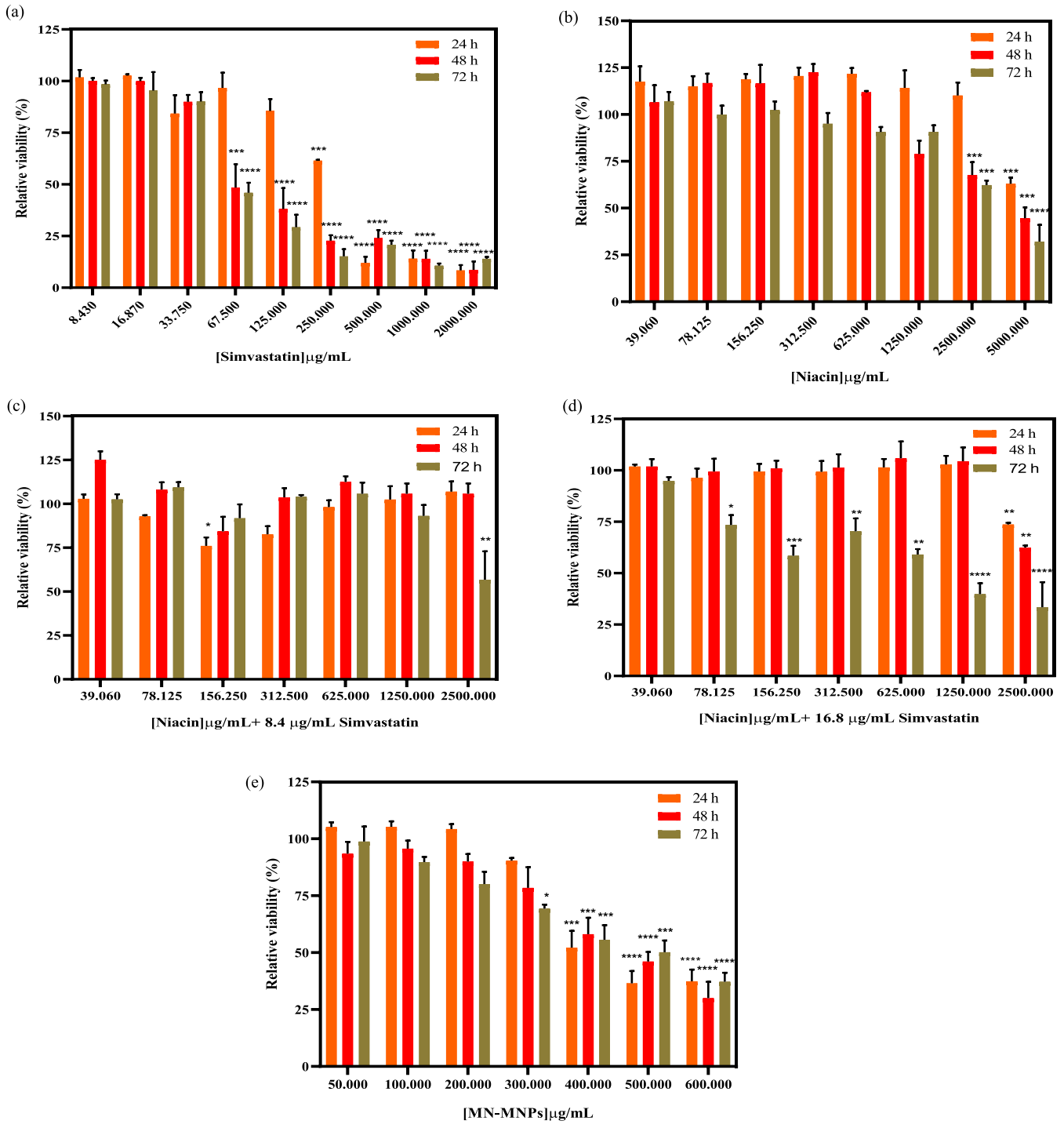


**Figure 3.** Toxicity analysis of (a) simvastatin and (b) niacin along with different concentrations of free niacin coupled with (c) 16.80 $\mu$g/mL and (d) 8.40 $\mu$g/mL of simvastatin on the J774A cell line at 24, 48, and 72 h. (e) Cellular toxicity of MN-MNPs at 24, 48, and 72 h of postincubation. All experiments were performed in three independent replicates, and the significance of changes was achieved using the one-way ANOVA (Kruskal–Wallis) method is defined as follows: * ($P \leq 0.05$), ** ($P \leq 0.01$), *** ($P \leq 0.001$), and **** ($P \leq 0.0001$).

refer to the C–H group in the MN polymer that is hardly detected in MN-MNP samples.

The XRD patterns of MN-MNPs are also presented in Figure 1c. Six characteristic peaks at $2\theta$ = 30.15, 35.60, 43.05, 54.55, 57.50, and 63.45° were observed that correspond to the diffractions of 220, 311, 400, 422, 511, and 440° crystal faces of the $Fe_3O_4$ spinel structure.

According to TEM analysis (see Figure 1d), the MN-MNPs exhibited a spherical shape with an inorganic core size of 15–25 nm and no detectable coating layer around which shows the small thickness of the mannan polymer shell. As illustrated in Figure 1e, the hydrodynamic size analysis was found to be 77.23 ± 13.90 nm, which is larger than the reported mannan-coated MNPs with 46.2 nm size.[28] The total net charge of the MNPs and MN-MNPs showed the relative shifts of $\zeta$ potential from negative (−30.1 ± 4.84 mV) to neutral (−4.24 ± 3.96 mV), which indeed proved the presence of mannan as a capping polymer on MN-MNPs.



https://doi.org/10.1021/acsomega.3c06389
ACS Omega 2024, 9, 658–674

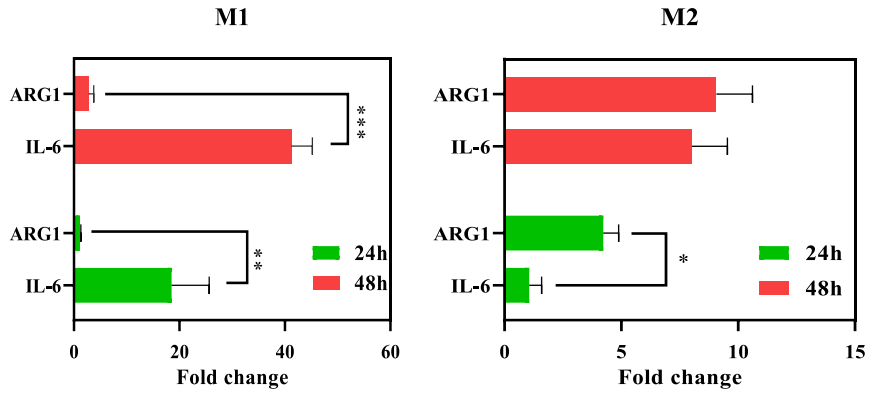


**Figure 4.** Macrophage polarization state with stimulus activation signals of *IL-6* and *ARG-1* expression levels. *** ($P \leq 0.001$) and **** ($P \leq 0.0001$).

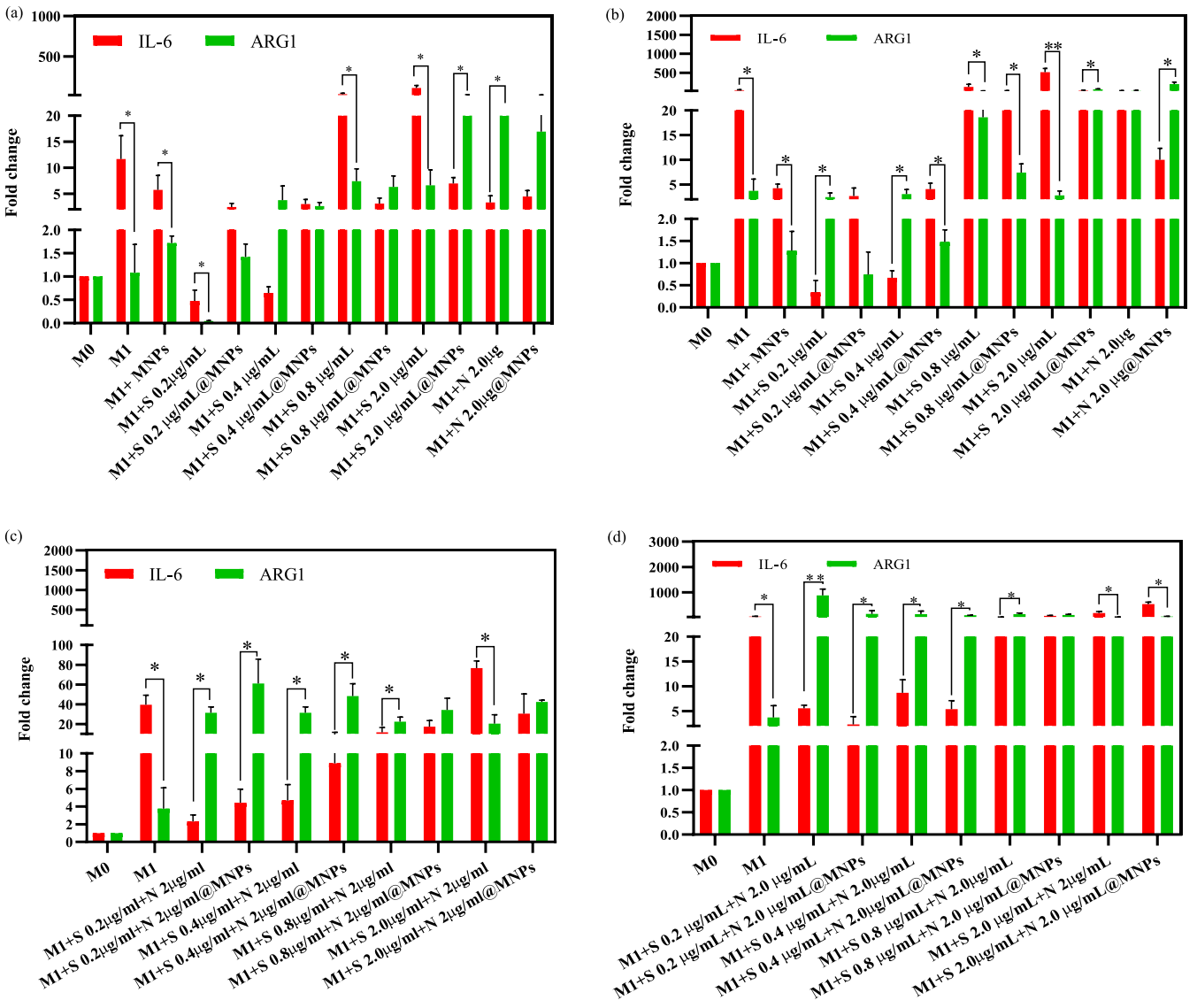


**Figure 5.** *IL-6* and *ARG1* expression levels after M1 stimulation with free and loaded MN-MNPs containing simvastatin, niacin, and simvastatin/niacin at (a,b) 24 and (c,d) 48 h postincubation. Significance of changes of the three independent replications was performed using one-way ANOVA (Kruskal–Wallis) method and is defined as follows: * ($P \leq 0.05$), ** ($P \leq 0.01$), *** ($P \leq 0.001$), and **** ($P \leq 0.0001$).

VSM research revealed that superparamagnetic NPs have been formed by MN-MNPs (Figure 1f). This is due to the sigmoid shape of the magnetic diagram reaching zero magnetic field. It was also determined that the magnetism of bare NPs is 60.01 emu $cm^{-3}$, and the mannan coating decreased the saturation level to 53.96 emu $cm^{-3}$.



https://doi.org/10.1021/acsomega.3c06389
ACS Omega 2024, 9, 658−674

**3.2. Drug Loading and Release.** The adsorption method was used to load the drugs onto NPs (Figure 2). The loading efficiency of drug absorption in the aqueous medium was up to 41.42 ± 0.8% (w/w) by adding NPs to a solution containing 2.0 mg/mL niacin. As simvastatin is poorly soluble in water and fails to load in water/methanol, the drug was gradually added to the PBS solution containing NPs. The simvastatin loading efficiency was calculated to be 75.36 ± 5.34 and 87.21 ± 3.7% (w/w) in N@MN-MNPs and MN-MNPs when using 6.0 mg/mL of simvastatin, respectively. The final loading capacity was estimated to be 20.11 ± 1.75% and 4.7 ± 0.3% (w/w) while using both niacin and simvastatin, respectively.

The simvastatin and niacin release kinetics was evaluated by the mannanase enzyme as a model enzyme substitute for lysosomal $\beta$-mannosidase with the help of simvastatin and niacin standard curves and distinct retention times (Figure S1). According to Figure 2a,b, the release rate of simvastatin and niacin in the presence of 0.02 mg/mL mannanase enzyme reached its maximum peak in 60 and 90 min, which was 67.23 and 79.51%, respectively. The unwanted diffusion rate (without using enzyme) was estimated to reach up to 19.22 and 14.38% after 90 min.

**3.3. Toxicity Assessment.** The cytotoxicity of niacin, simvastatin, niacin/simvastatin, and also MN-MNPs was tested against J774A murine macrophages, and the results are presented in Figure 3. As illustrated in Figure 3a, the cytotoxicity trend of free simvastatin on macrophage cells was time dependent with a safe borderline up to 33.75 $\mu$g/mL for 72 h. The niacin treatment showed different trends on murine macrophages, which displayed growth in concentrations up to 625 $\mu$g/mL at 24 and 48 h of post-treatment (see Figure 3b). The safe borderline of niacin treatment is expected to be up to 1250 $\mu$g/mL. The cell toxicity evaluation in the presence of constant concentrations of simvastatin and different concentrations of niacin indicates that up to a constant concentration of 8.4 $\mu$g/mL (equal to 20 $\mu$M) simvastatin and niacin, up to 1250 $\mu$g/mL is relatively safe for cellular treatment (see Figure 3c,d). Additionally, J774A cellular incubation of the MN-MNPs at concentrations below 200 $\mu$g/mL was relatively safe for treatment up to 72 h (Figure 3e).

**3.4. J774A Polarization and Treatment.** The polarization of J774A was determined using the fold change expression of interleukin 6 (*IL-6*) and arginase 1 (*ARG1*) genes as M1 and M2 biomarkers against beta−actin, respectively. As illustrated in Figure 4, the optimal concentrations of LPS, IFN-$\gamma$, and IL-4 for M1 and M2 macrophage polarization were 100.0 ng/mL, 50.0 $\mu$g/mL, and 5.0 $\mu$g/mL, respectively. The expression levels of M1 (*IL-6*) and M2 (*ARG1*) marker genes were assessed on M1 prestimulated J774A cells after 24 and 48 h of post-treatment with different concentrations of simvastatin (0.2−2.0 $\mu$g/mL), niacin (2.0 $\mu$g/mL), and simvastatin/niacin (0.2−2.0/2.0 $\mu$g/mL) and also S@MN-MNPs (0.2−2.0 $\mu$g/mL), N@MN-MNPs (2.0 $\mu$g/mL), and S + N@MN-MNPs (0.2−2.0/2.0 $\mu$g/mL) (see Figure 5). According to Figure 5a, treatment of polarized M1 cells with 0.2 $\mu$g/mL of simvastatin had a significant inhibitory effect ($P$ = 0.028) on the expression levels of both M1 and M2 markers. Treatment of the cells with moderate concentration of simvastatin (0.4 $\mu$g/mL) led to shift of the M1 to M2 subset ($p$ = 0.028). The effect of simvastatin at high concentrations (0.8 and 2.0 $\mu$g/mL) led to a significantly higher expression of *IL-6* ($P$ = 0.004 and 0.028) and thus created more M1-polarized macrophage subset.[47] Also, as shown in Figure 5b, after 48 h of the treatment, the stimulation trend of cells was similar to that of the 24 h treatment, except that the expression of *IL-6* was far higher than 24 h in moderate and high simvastatin concentrations ($p$ = 0.028 and 0.014).

Also, according to Figure 5a,b, 24 h of free niacin administration on M1 macrophages showed a significant shift of M1 to M2 subset ($P$ = 0.028), but over time, *IL-6* induction led to mixed population of M1/M2 ($P$ > 0.05). The effect of S@MN-MNPs on the M1 subset after 24 and 48 h of incubation showed a reduced *IL-6* expression compared to simvastatin. Even the use of concentrations as low as 0.2 $\mu$g/mL of simvastatin reduced the expression of both *IL-6* and *ARG1* up to 48 h, which may indicate the formation of a mixed M1/M2 population. Moderate doses of S@MN-MNPs (0.4 $\mu$g/mL) showed a slightly increasing trend of M2 biomarkers, albeit the long-term exposure effects have led the population to retain the M1 polarization. S@MN-MNP treatment in high concentrations (0.8−2.0 $\mu$g/mL) displayed a significant increase in the expression of the *ARG1* gene (M2 biomarker, $P$ = 0.028), which was enhanced after 48 h of treatment. Similar to free treatment of simvastatin, the *IL-6*-stimulated expression of S@MN-MNP showed a time-dependent trend and led to generate the M1/M2 macrophage subsets; nevertheless, *ARG1* gene expression in the S@MN-MNP was far higher than that of free simvastatin administration.

The effect of N@MN-MNPs at 24 and 48 h of incubation is also shown in Figure 5a,b. The effect of N@MN-MNPs on the M1-induced macrophage reduced *IL-6* expression and significantly increased *ARG1* ($P$ = 0.028) after 48 h post-treatment. Similar to free treatment of niacin, the *ARG1* levels were elevated slowly up to 48 h. Also, the cotreatment of simvastatin/niacin on M1-stimulated macrophage cells for 24 and 48 h was evaluated. Therefore, the administration of the maximum safe concentration of niacin along with different concentrations of simvastatin at low and moderate concentrations (0.2 and 0.4 $\mu$g/mL, $P$ = 0.028 and 0.004) successfully induced M1 to M2 subsets at 24 and 48 h post-treatment. By increasing the concentration of simvastatin to 2.0 $\mu$g/mL, this process increased the expression of *IL-6*, resulting in mixed M1 and M2 populations both 24 and 48 h post-treatments. Moreover, treatment of cells with simvastatin/niacin caused a significant induction of *ARG1* ($P$ = 0.028) in a time-dependent manner process.

The effect of S + N@MN-MNPs at 24 and 48 h incubation times is also shown in Figure 5c,d. Short-term administration of S + N@MN-MNPs at 0.2 $\mu$g/mL of simvastatin showed a temporary elevation of *IL-6* expression that is probably due to the presence of mannan NPs. Treatment of high concentrations of simvastatin/niacin and S + N@MN-MNPs on *IL-6* expression displayed a concentration- and time-dependent manner. This means that the use of concentrations higher than 0.4 $\mu$g/mL of simvastatin produced a mixture of M1/M2 subsets of macrophages, and this process was associated with a severe increase in *IL-6* expression in the M1 subset when using 2.0 $\mu$g/mL simvastatin ($P$ = 0.028). The expression of the *ARG1* gene in S + N@MN-MNPs showed a decreasing trend with increasing simvastatin concentration over time. Therefore, we concluded that the appropriate concentration for the treatment of both free and encapsulated forms was 0.4 and with 2.0 $\mu$g/mL simvastatin and niacin, respectively.


https://doi.org/10.1021/acsomega.3c06389
ACS Omega 2024, 9, 658−674

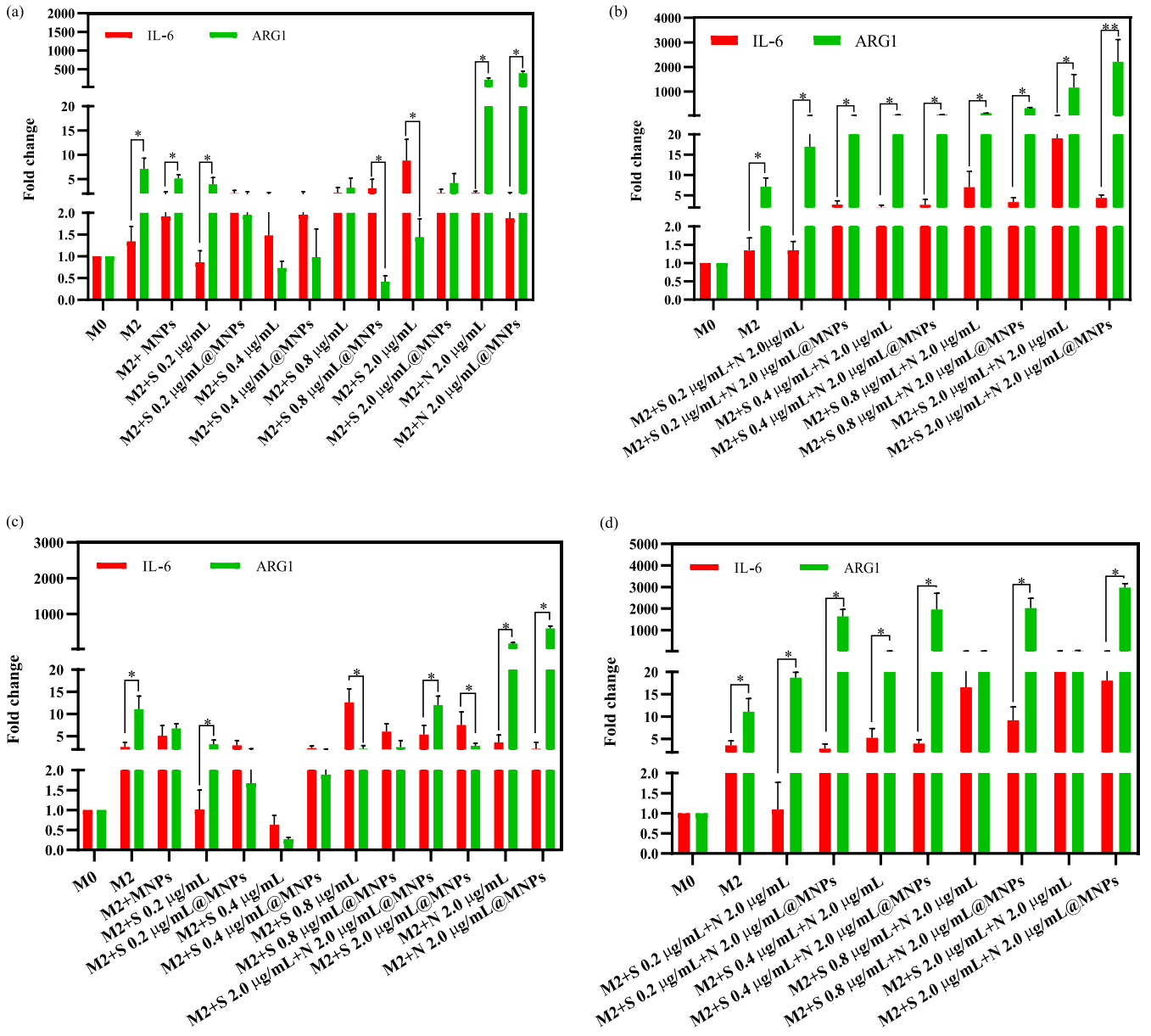


**Figure 6.** *IL-6* and *ARG1* expression levels after M2 stimulation with free and loaded MN-MNPs containing simvastatin, niacin, and simvastatin/niacin at (a,c) 24 and (b,d) 48 h postincubation. Significance of changes of the three independent replications was performed using one-way ANOVA (Kruskal–Wallis) method and is defined as follows: * ($P \leq 0.05$), ** ($P \leq 0.01$), *** ($P \leq 0.001$), and **** ($P \leq 0.0001$).

The effect of simvastatin, niacin, and simvastatin/niacin as well as S@MN-MNPs, N@MN-MNPs, and S + N@MN-MNPs on M2-stimulated J774A macrophage was also investigated. As shown in Figure 6a, treatment of M2 macrophages with different concentrations of simvastatin (0.2–2.0 $\mu$g/mL) showed that at low and moderate concentrations of simvastatin (0.2 and 0.4 $\mu$M), a slight but nonsignificant suppression effect was detected on M2 marker, *ARG1*, and gene expression ($P > 0.05$). The decreasing trend in the expression levels of the M1 biomarker, *IL-6*, at low concentrations (0.2 and 0.4 $\mu$g/mL) was seen, although the significant induction of *IL-6* was detected when using high simvastatin concentrations (0.8 and 2.0 $\mu$g/mL, $P = 0.028$), which reflect the inflammatory subset shift in M2 macrophage populations. Long time exposure to low concentrations of simvastatin (0.2 and 0.4 $\mu$g/mL) exhibited a similar inhibitory trend on both M1 and M2 biomarkers. Remarkably, similar to 24 h post-treatment, a significant shift from of M2 to M1 subset was detected at high concentrations ($P = 0.028$). It should be mentioned that the expression level of both markers was higher in 48 h under the influence of high concentrations of simvastatin, which indicates the fact that the response of M2 cells to simvastatin treatment happens a time-dependent manner, especially for *ARG1* gene expression.

Also, according to Figure 6a,b, the effect of free treatment of niacin on the M2-polarized macrophage demonstrated that after 24 h of treatment, macrophages significantly shifted into the M2 subset ($P = 0.028$), and this trend lasted to the end of the experiment at 48 h ($P = 0.028$). S@MN-MNPs in 24 h incubation with the M2-polarized macrophage significantly increased *IL-6* expression levels ($P = 0.028$). However, after 48 h, *IL-6* expression levels did not show any significant changes ($P > 0.05$). Overall, the statistical analysis of S@MN-MNP treatment results showed that the use of 0.2 and 0.4 $\mu$g/


https://doi.org/10.1021/acsomega.3c06389
ACS Omega 2024, 9, 658–674

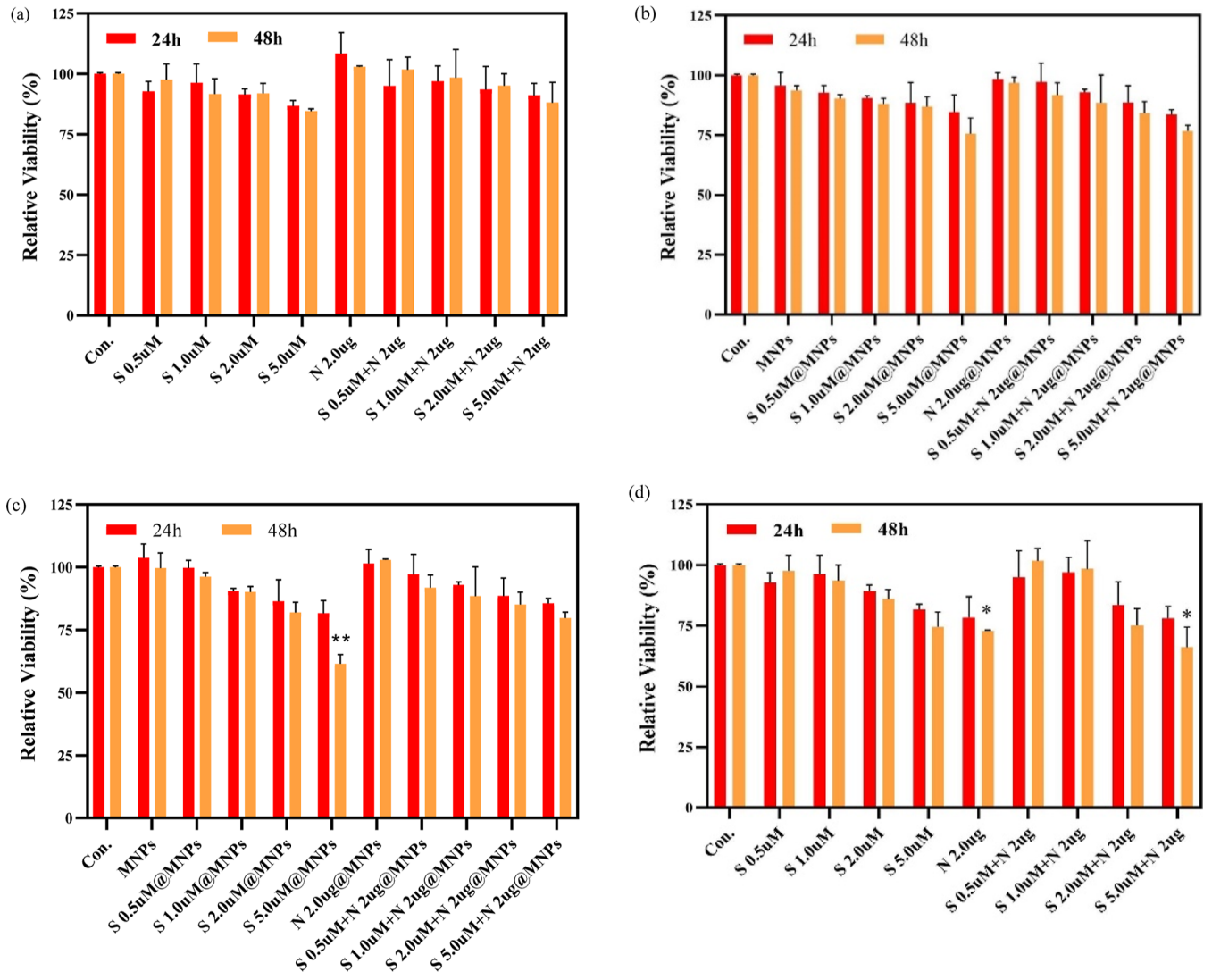


**Figure 7.** Toxicity analysis of free simvastatin, niacin and simvastatin/niacin and simvastatin, and niacin and simvastatin/niacin loaded on 100 $\mu$g/mL MN-MNPs on (a,b) HUVECs, (c) normal liver cells at 24 h, and (d) normal liver cells at 48 h was investigated. All experiments were presented as average of three independent replicates. Significance of changes of the three independent replications was performed using the one-way ANOVA (Kruskal–Wallis) method and is defined as follows: * ($P \leq 0.05$), ** ($P \leq 0.01$), *** ($P \leq 0.001$), and **** ($P \leq 0.0001$).

mL of simvastatin reduced the expression levels of *IL-6* and *ARG1*, which lasted for 48 h. In the S@MN-MNP treatment at moderate concentrations, the anti-inhibitory effect on *IL-6* gene over 48 h ($P > 0.05$) indicates gradual release of the drug from the scaffold and consequently decline of macrophage induction. Similar to the case of the free simvastatin, the effect of S@MN-MNP treatment on *IL-6* expression levels showed a time-dependent manner. Also, induction of the *IL-6* and *ARG1* expression at high-dose treatment (2.0 $\mu$g/mL) showed a time-dependent manner so that after 48 h, a mixture of both subsets of M1 and M2 was detectable. The effect of N@MN-MNPs at 24 and 48 h post-treatment is also shown in Figure 6a,b. The administration of encapsulated niacin on M2-polarized macrophage diminished the *IL-6* expression levels and significantly increased *ARG1* ($P = 0.028$) at both 24 and 48 h after treatment. Similar to the free-drug state, after 48 h of treatment with N@MN-MNPs, a significant increase in *ARG1* expression can be seen ($P = 0.028$).

According to Figures 6c,d, the treatment of M2-polarized cells with simvastatin/niacin at 24 and 48 h was evaluated. The maximum safe concentration of niacin along with different concentrations of simvastatin significantly increased the expression of *ARG1* at all concentrations (P = 0.028). This trend was observed at low concentrations (0.2 and 0.4 $\mu$g/mL) in 24 h, whereas after treatment with free simvastatin at a concentration of 0.4 $\mu$M for 48 h, the *IL-6* expression increased dramatically. These results indicated that the use of simvastatin, either alone or concomitantly with niacin up to a concentration of 0.4 $\mu$g/mL, significantly induced *ARG1* expression. Moreover, niacin/simvastatin combination treatment at higher concentrations of simvastatin (>0.4 $\mu$g/mL) increased *IL-6* expression at both 24 and 48 h, which subsequently increased the shift to the M1 subset, resulting in M1/M2 mixture when using 2.0 $\mu$g/mL of simvastatin. A decreasing trend in *ARG1* expression levels can be seen in 48 h postexposure to simvastatin/niacin. Also, as shown in Figure 6c,d, treatment of J774A cells with free simvastatin/niacin induced *ARG1* expression in a time-independent manner. The effect of 24 and 48 h post-treatment of equal concentrations of free simvastatin/niacin as well as S + N@MN-MNPs, on


https://doi.org/10.1021/acsomega.3c06389
ACS Omega 2024, 9, 658−674

M2-polarized cells, is shown in Figure 6d. After 24 h treatment of the M2-polarized subset with 0.2, 0.4, and 0.8 $\mu$g/mL of simvastatin/2.0 mg/mL niacin, a significant elevation in *ARG1* gene expression can be seen ($P$ = 0.028), while in the case of *IL-6* expression, a decreasing trend was observed compared to the free formulation at higher concentrations. Treatment of high concentrations of S + N@MN-MNPs on *IL-6* and *ARG1* expression levels showed a concentration- and time-dependent manner. Therefore, the use of concentrations higher than 0.8 $\mu$g/mL led to an increase in *IL-6* expression, but the increase was less than in the free-state treatment with simvastatin ($P$ > 0.05). As a result, the appropriate concentration for codelivery system treatment of both free and encapsulated forms was estimated to be 0.2 and 0.4 $\mu$g/mL, respectively, of simvastatin along with 2.0 mg/mL of niacin.

**3.5. Cellular Toxicity.** The side effects of simvastatin, niacin, and simvastatin/niacin formulations on HUVECs as well as normal liver cells were evaluated using MTT and apoptosis/necrosis assay. As illustrated in Figure 7a,b, the MTT results showed that administration of free and encapsulated formulations of niacin and simvastatin/niacin did not show a significant effect on HUVECs. Short-term treatment of HUVECs with variable amounts of simvastatin (0.2−2.0 $\mu$g/mL) also did not cause significant toxicity, while within 48 h, a significant toxicity was observed in S@MN-MNPs at a concentration of 2.0 $\mu$g/mL.

As shown in Figure 7c,d, free administration of niacin and simvastatin/niacin formulations resulted in liver cell toxicity after longer exposure, while the nanoformulation of niacin and niacin/simvastatin did not show significant toxicity at a similar time point. Therefore, it can be concluded that the administration of these formulations did not cause any unwanted side effects in the short-term period. Treatment of normal liver cells with high levels of simvastatin and niacin showed a destructive effect on cells, while encapsulation of the drugs in mannan NPs and their controlled release reduced the toxicity. Therefore, according to the present experiment, the use of NPs containing simvastatin, niacin, and simvastatin/niacin on liver cells did not cause any adverse effects on hepatic cells.

The effect of free and encapsulated simvastatin, niacin, and simvastatin/niacin delivery on J774A cells, HUVECs, and normal liver cells were analyzed using flow cytometry (see Figures S2−S7). As illustrated in Figure S2, treatment of J774A macrophage cells with simvastatin at high concentrations induced apoptosis by 27.4% (Figure S2a,b), while the effect of niacin showed no detectable toxicity (Figure S2c). The codelivery effect of simvastatin/niacin modulated the apoptosis-mediated cell death in macrophages (Figure S2d). Also, the treatment of the J774A macrophage cell line with the targeted formulations using mannan NPs induced a slight necrosis in cells (Figure S3b). However, S@MN-MNPs increased the rate of apoptosis up to 7.3% (Figure S3c). On the contrary, the apoptotic effect of niacin on J774A cells was negligible (Figure S3d). The codelivery of simvastatin/niacin on the J774A cell line modulated the induction of apoptosis in the cells (Figure S3e).

Treatment with simvastatin at high concentrations slightly induced the apoptosis process in HUVECs (Figure S4a,b), while the apoptosis-induced trend was negligible in the treatment of niacin (Figure S4c). The codelivery of simvastatin/niacin on the HUVEC line further reduced the induction of apoptosis (Figure S4d). The effect of S@MN-MNPs, N@MN-MNPs, and S + N@MN-MNPs on HUVECs is shown in Figure S4. The MN-MNPs did not show a significant negative effect on HUVECs; however, S@MN-MNPs increased the rate of apoptosis up to 19.7% (Figure S5a−c). The apoptotic effect of niacin on HUVECs was very small, and the codelivery effect of simvastatin/niacin modulated apoptosis compared to niacin treatment (Figure S5d,e). As shown in Figure S6a,b, treatment of normal hepatic cells with simvastatin at high concentrations induced slight apoptosis. In contrast, the free treatment with niacin showed a high rate of apoptotic cell death up to 19.9% (Figure S6c). The codelivery of simvastatin/niacin slightly reduced the apoptosis induction in hepatocytes (Figure S6d). The effect of S@MN-MNPs, N@MN-MNPs, and S + N@MN-MNPs on normal hepatic cells is shown in Figure S7. The MN-MNPs showed a slight negative effect on the induction of necrosis (see Figure S7a,b). The S@MN-MNP treatment displayed a reduced apoptosis rate in hepatic cells (Figure S7c). The apoptotic effect of niacin on hepatic cells was negligible, and the codelivery of S + N@MN-MNPs modulated the apoptosis trend compared to simvastatin/niacin and niacin (Figure S7d,e).

Overall, the results of cell death studies in three cell lines, J774A, HUVEC, and normal liver, are summarized in Figure 8. As shown in Figure 8a, free simvastatin resulted in significant cell death of J774A macrophage cells ($P$ = 0.012), which was not seen when using S@MN-MNPs ($P$ = 0.914). This may partly be due to the controlled release of simvastatin from S@MN-MNPs. Treatment with niacin ($P$ = 0.925) and niacin/simvastatin ($P$ > 0.999), MN-MNPs ($P$ > 0.999), N@MN-MNPs ($P$ > 0.999), and S + N@MN-MNPs ($P$ = 0.923) did not show a significant effect on J774A cells. Importantly, nonparametric $t$-test (Mann−Whitney) analysis showed that the treatment of J774A cells with free formulation of simvastatin did not increase necrotic cell death ($P$ = 0.914), while it induced significant apoptosis in the cells ($P$ = 0.002). Other treatments did not show a significant effect on the induction of apoptosis in J774A cells. Interestingly, treatment with S + N@MN-MNPs significantly reduced apoptosis in J774A cells ($P$ = 0.046).

As shown in Figure 8b, simvastatin treatment resulted in nonsignificant cell death in HUVECs compared to the control ($P$ = 0.502). The S@MN-MNPs resulted in a slight decrease in apoptosis ($P$ > 0.999). Treatment of HUVECs with niacin ($P$ > 0.999) and N@MN-MNPs ($P$ > 0.999) did not show any significant effect on induction of cell death compared to the control. MN-MNPs also did not induce significant cell death in HUVECs compared to the control ($P$ > 0.999). The niacin/simvastatin formulation ($P$ > 0.999) and S + N@MN-MNPs ($P$ > 0.999) also did not show a significant change in the induction of cell death compared to the control. Also, it should be mentioned that S + N@MN-MNP formulation did not show a significant reduction in cell death (apoptosis and necrosis) compared to the free drug formulations ($P$ = 0.999).

As shown in Figure 8c, simvastatin ($P$ > 0.999), S@N-MNPs ($P$ > 0.999), niacin ($P$ = 0.061), and N@MN-MNP treatment ($P$ = 0.131) did not induce significant cell death in normal liver cells. However, coadministration of niacin/simvastatin significantly increased cell death in normal liver cells ($P$ = 0.009). The S + N@MN-MNP formulation significantly reduced the induction of cell death in normal liver cells ($P$ = 0.031). Based on the results, free


https://doi.org/10.1021/acsomega.3c06389
ACS Omega 2024, 9, 658−674

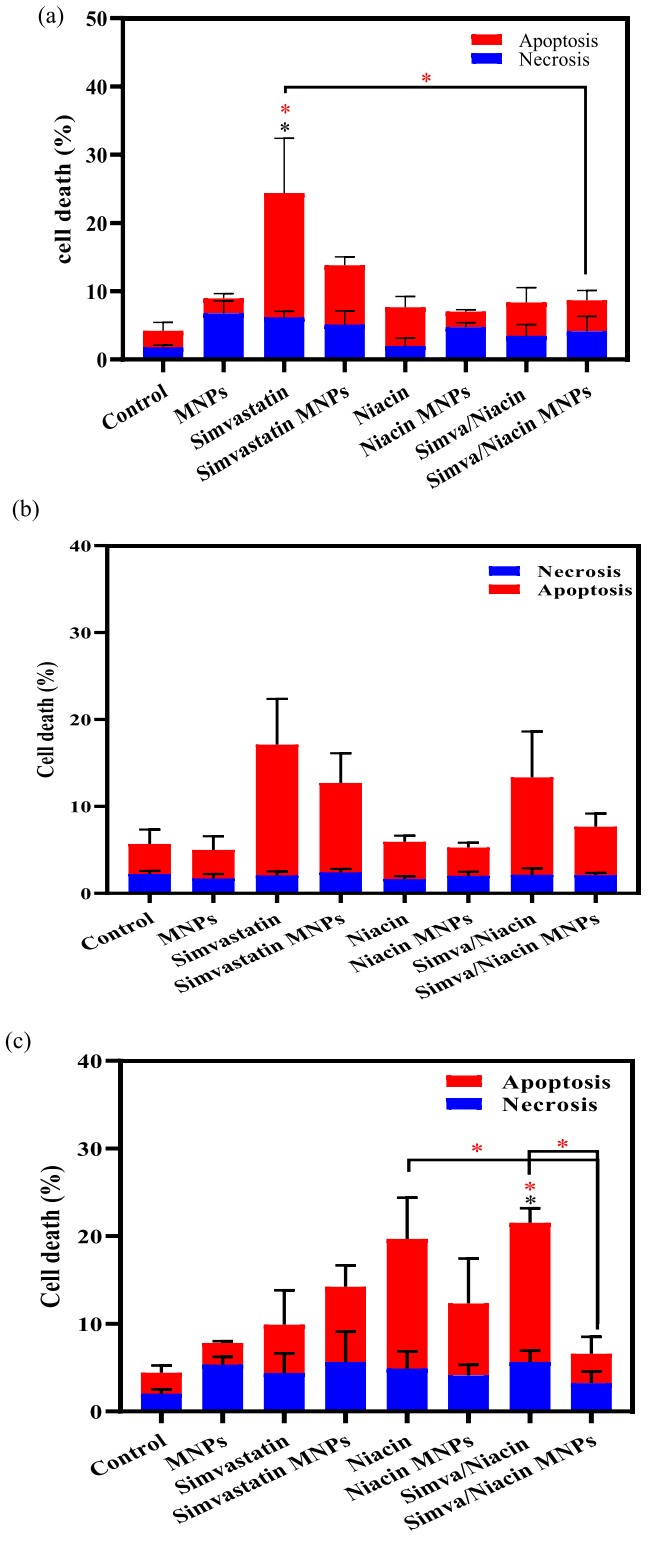


**Figure 8.** Toxicity analysis of free and encapsulated formulations on MN-MNPs by flow cytometry on (a) J774A, (b) HUVEC, and (c) normal liver cells with 2 $\mu$g/mL simvastatin, 2 $\mu$g/mL niacin, and 2 $\mu$g/mL simvastatin/2 $\mu$g/mL niacin. The black stars represent the results of *t*-test analysis (Mann−Whitney), and the red stars show the one-way ANOVA (Kruskal−Wallis) analysis. Significance of changes of the three independent replications was performed and is defined as follows: * ($P \leq 0.05$), ** ($P \leq 0.01$), *** ($P \leq 0.001$), and **** ($P \leq 0.0001$).

administration of niacin/simvastatin led to a significant increase in apoptosis in normal liver cells compared to the control treatment ($P = 0.043$). Also, codelivery of S + N@MN-MNPs showed a strong reduced effect on apoptosis induction compared to the free formulation ($P = 0.019$). Moreover, compared to niacin treatment, controlled codelivery of S + N@MN-MNPs showed a significant reduction of apoptosis in normal liver cells ($P = 0.028$).

## 4. DISCUSSION

In the first part of this study, we successfully synthesized enzyme-sensitive magnetic NPs coated with mannose polymer to carry medications and be targeted to mannose receptors on macrophages as a key player in atherosclerosis.

Characterization of functional group of MN-MNPs by the FT-IR spectrum at 400−4000 $cm^{-1}$ wavenumber showed the presence of O−H groups in the range of 3419 $cm^{-1}$, C−H group in the range of 12,927 and 2867 $cm^{-1}$, C−C bond in the range of 11,640−1630 $cm^{-1}$, and C−O bond in the range of 1070 $cm^{-1}$, which represented the corporation of sugar polymer in MN-MNPs. Also, the presence of Fe−O bond in the coated NPs was significant, which all indicate the presence of magnetite NPs within the mannan polymer.[27] X-ray diffraction (XRD) technique was used to evaluate the purity of magnetic NPs and the quality of mineralization. The presence of six peaks in the $2\theta$ regions at 30.15, 35.60, 43.55, 54.55, 57.50, and 63.45° indicated the formation of octagonal cube diffraction of $Fe_3O_4$ structures (220, 311, 400, 422, 511, and 440°). The correct positions and intensities of the reflection peak of all MNPs agree with the XRD diffraction peaks of reported $Fe_3O_4$,[48] and sharp peaks indicated good crystallization. These characteristics correspond to the arrangement of the obtained spectra with those mentioned in earlier reports, and also the height and sharpness of the peaks indicated the proper crystallization of the NPs.[48] The small decrease in peak intensity and the increase in spectrum disturbance are due to the presence of amorphous polysaccharide structures.[49] Therefore, it can be said that the NPs synthesized by the single-step method are magnetite NPs ($Fe_3O_4$), and the polysaccharide coating was relatively thin so that it did not have a significant effect on the sharpness of $Fe_3O_4$ crystal structure.

According to TEM analysis, our MN-MNPs exhibited a well-crystallized spherical shape with an inorganic core size of 15−25 nm and a thin encircled coating layer, which shows the small thickness of the mannan polymer shell. The ability to cross-natural biological barriers is largely related to the physicochemical properties of NPs, including morphology, hydrodynamic size, charge, and other surface properties.[50,51] Particle size is relatively critical for targeted drug delivery that dictated several criteria such as their circulation in the blood, shelf life, tissue accumulation, cellular uptake, and subcellular distribution.[52] The hydrodynamic size of NPs can have a great impact on how they behave in clinical settings. While NPs less than 5 nm are immediately cleared by kidney infiltrations,[53,54] medium-sized NPs (30−150 nm) are capable of accumulating in organs like bone marrow, heart, kidney, and stomach. Large NPs (150−300 nm) are mainly entrapped with phagocytic systems which finally accumulates in the liver and spleen.[55] Several studies conducted so far mentioned that NPs with a size of 50−100 nm can persist in the bloodstream for up to 2 h, and hydrophilic NPs smaller than 200 nm can easily escape from phagocytosis due to their lack of interaction with plasma


https://doi.org/10.1021/acsomega.3c06389
ACS Omega 2024, 9, 658−674

proteins.[30,56] Different studies have shown that the renal filtration and liver entrapment NPs' cutoff size is 5.5 and 50 nm, respectively.[57,58] Besides, the leaky vasculature, called the EPR effect, in atherosclerotic lesions helps NPs to pass into the plaque region more efficiently, while an undeveloped lymphatic drainage system increases the local concentration of NP-carrying drugs.[59] The hydrodynamic size of MN-MNPs was estimated to be 77.23 ± 13.90 nm, which is larger than that of the reported mannan coated-MNPs (46.2 nm).[28] The size difference between TEM and DLS analyses may be related to the swelling ability of the polysaccharide polymers in a liquid medium. Therefore, it can be predicted that MN-MNPs are relatively able to maintain in blood and capable of escaping from phagocytosis. NP cores with minor size (<30 nm) have superparamagnetic properties which need to be improved to avoid aggregation in vivo.[60] In other words, the superparamagnetic properties of magnetite help the delivery system to response to the magnetic field when using external magnet and stop the magnetization of the NPs immediately once removed from the magnetic field.[61] The VSM analysis was performed to confirm the magnetic properties of MN-MNPs which were further classified as superparamagnetic NPs due to the sigmoid shape of the magnetic diagram and reaching zero magnetism.[30] The thickness of the carbohydrate polymer is capable of weakening the magnetic saturation state compared to the uncoated MNPs. According to the VSM analysis of bare MNP (data not shown) and MN-MNPs, the saturation curve is reduced from 60.01 to 53.96 $cm^{-3}$ emu. Also, the closeness of the magnetic saturation of MN-MNPs and MNPs is the sign of the least crystalline irregularity in the NPs.[62] The surface charge of NPs also plays an important role in preventing unwanted interactions with other macromolecules, cell adsorption, and cell targeting in heterogeneous environments such as blood and interstitial fluid.[63] The surface charge of MNPs was determined to be a strong negative charge (−26.67 mV), which is due to the presence of OH groups on the NP surface. Coating of NPs with mannan polymer changed this value to a neutral area at −4.24 mV. The change in $\zeta$ potential can also indicate the successful coating of the magnetic NPs with the polymer. Near-neutral $\zeta$ potential helped out the NPs to prevent any unwanted electrostatic interactions with other biomolecules in the plasma.[64]

In the second part of the study, we loaded the NPs with simvastatin and niacin to target these commonly used medicines to M1 and M2 macrophages in vitro and evaluated their toxicity and impacts on the cells. The drug loading efficiencies of niacin and simvastatin were calculated to be 87.21% and 75.36%, respectively, which is more than the loading rate of other reported substrates such as the PLGA-coated substrate with an efficiency of 24.8% for Paclitaxel and in the range of substrates such as chondroitin sulfate A with 85% efficiency for doxorubicin loading and chitosan-$\beta$-cyclodextrin substrate with 88% loading efficiency for curcumin.[65−67] The loading capacity of niacin, simvastatin, and niacin/simvastatin on MN-MNPs was calculated to be 21.15−5.03%, which is an acceptable amount to affect macrophage cells. Given that drug release by endocytosis is one of the most effective strategies for drug delivery to the target cell, the use of substrates sensitive to lysosomal enzymes is a convenient way to release therapeutic drugs. To determine the enzyme-mediated release of MN-MNPs, S@MN-MNPs and N@MN-MNPs were prepared, and the drug release behavior in the medium containing 1 mg/mL BSA in the presence and absence of coating mannose hydrolyzing enzymes to simulate lysosomal degradation and bloodstream was evaluated. The unwanted leakage of niacin and simvastatin in N@MN-MNPs and S@MN-MNPs is calculated to be 19.22 and 14.38, which is much lower than previously reported scaffolds such as magnetic chitosan micelles with 65% release and pectin magnetic NPs with 60 and 34% release, respectively. The reported leakage in other nanocarriers like Chitosan@$\beta$-cyclodextrin (30%) and Ca-Gly-Maltose-D16F7 (25%) was also higher than our delivery system.[66,68−70] The enzyme-mediated release of niacin and simvastatin was estimated to be 67.23 and 79.51%, respectively. In our delivery system, active lysosomal enzymes, $\alpha$-D-mannosidase, are predicted to act as a polymer degrading agent. There are limited reports on the enzyme-sensitive drug delivery systems, and most importantly, pH-sensitive release is between 30 and 90%.[71] The doxorubicin releasing profile from $\beta$-cyclodextrin NPs, simvastatin release from Ca-Gly-Maltose-D16F7, and methotrexate from pectin NPs at pH = 5 was reported to be 37, 54, and 90%, respectively which are comparable with our system.[68,72,73]

The use of biocompatible NPs is favorable with the aim of increasing drug uptake efficiency, reducing unwanted side effects, and preventing premature drug release. We used macrophages, HUVECs, and hepatocytes for biocompatibility experiments. Macrophages possess the ability to either mediate or suppress inflammatory responses based on their cytokine secretion pattern and cellular phenotype. However, treatments of autoimmune diseases, early stage of cancer and tissue regeneration, may benefit substantially from macrophage switching from an inflammatory (M1) to anti-inflammatory (M2) phenotype; this may not be the case in late stages of cancer.[74] Similarly, M1 and M2 macrophages play different roles in different stages of atherosclerosis, but when the plaque is formed and developed, which is when the angiography can help in risk assessment, M2 macrophages are advantageous.[34] Therefore, overcoming the M1 (inflammatory) phenotype and evolving into the M2 (anti-inflammatory) phenotype are of substantial benefit. The biocompatibility assessments of the MN-MNPs at concentrations ranging from 50 to 600 $\mu$g/mL against J774A cells revealed the usage safety of NPs up to 200 $\mu$g/mL even in 72 h of incubation.

To be more specific, after successful treatment of macrophages with LPS/IFN-$\gamma$ and IL-4 to induce M1 and M2 deviation, the effects of simvastatin, niacin, and simvastatin/niacin combination as well as S@MN-MNPs, N@MN-MNPs, and S + N@MN-MNPs on expression levels of M1 (*IL-6*) and M2 (*ARG1*) marker genes were investigated. Free simvastatin reduced *IL-6* in LPS/IFN-$\gamma$-stimulated (M1) macrophages at low concentrations (0.2 and 0.4 $\mu$g/mL). Free administration of simvastatin at high doses caused a time-dependent increased expression of *IL-6* which may accelerate progression of atherosclerosis in vivo. Therefore, free simvastatin shifted macrophages from the M1 to M2 subsets only at low concentrations. The MN-MNP nanocarrier showed a negative trend in *IL-6* expression. Interestingly, the S@MN-MNPs modulated the inflammatory effect of the LPS/IFN-$\gamma$-induced M1 macrophage subset. In general, our results are consistent with an earlier study in which simvastatin treatment at concentrations of 1.7−8.8 $\mu$M (equal to 0.68 to 3.52 $\mu$g/mL) resulted in short time (9 h),


https://doi.org/10.1021/acsomega.3c06389
ACS Omega 2024, 9, 658−674

increased expression levels of CD206, and significant IL-10 secretion, as indication of M1 to M2 shift.[75]

We showed that short-term (24 h) niacin treatment of M1 macrophages had a positive effect on *ARG1* expression and thus showed a significant shift from M1 to M2 populations. The long-time exposure of M1 macrophages to niacin (48 h) led to an increase in markers associated with both M1 and M2 populations. However, due to controlled drug release, the N@MN-MNP treatment had a positive and continuous trend from M1 to M2 in the long-term exposure. Therefore, it can be concluded that compared to free administration of niacin, long-term treatment of N@MN-MNPs has a stronger effect on induction of M2 macrophages, which are considered anti-inflammatory and in favor of plaque stability in vivo. Similarly, in an earlier study on healthy human M1 macrophages and mice with metabolic syndrome, niacin treatment was capable of shifting M1 macrophages to M2 populations.[76,77] Niacin mainly affects the cells through a hydroxycarboxylic acid receptor 2, the so-called HCAR2 or GPR109A. Several studies have shown that niacin may play an anti-inflammatory role in diseases such as Parkinson's via GPR109A/HCA2, which is highly expressed in adipose tissue and macrophages.[78−80] Studies suggest that Gpr109a signaling may induce anti-inflammatory properties in macrophages and dendritic cells, enabling them to differentiate between Treg cells and IL-10-producing T cells.[81] Interaction with GPR109A may reduce the NF-κB signaling pathway and antioxidant mechanisms and amplify mitochondrial NAD, which may explain how macrophage polarization occurs under the M2 populations.[82] Apparently, similar to the role of macrophages in Parkinson's disease, in the current study, the effect of niacin on induced macrophages has shown an anti-inflammatory effect in the short- and long-term (24 and 48 h) treatment through increased M2 marker, *ARG1*, expression levels.

The effect of S + N@MN-MNPs on M1 macrophage populations indicated that treatment at low simvastatin concentrations (0.2 μg/mL) led to a significant shift from M1 to M2 populations. However, both short- and long-term exposure to moderate and high concentrations of simvastatin alone increased M1 polarization and the mixture of M1/M2 macrophages. The short time (24 h) effect of S + N@MN-MNPs (0.2−0.4 μg/mL) had a similar effect to the free formulation, but in the long term, due to controlled drug release, a sharp decrease in the inflammatory M1 marker, *IL-6*, and a significant increase in the anti-inflammatory marker, *ARG1*, were detected, which confirmed a shift in M1 to M2 populations. Increasing the concentration of simvastatin in S + N@MN-MNPs not only increased the expression of inflammatory marker *IL-6* but also had an inhibitory effect on the expression of *ARG1* compatible with the activation of macrophages, which can have a stimulatory effect on plaque progression. Altogether, it can be said that the use of high doses of simvastatin and S@MN-MNPs (>0.8 μg/mL) is not only inappropriate but can also help the progression of atherosclerotic plaque in the early stages of plaque formation. Administration of niacin alone or in combination with low concentrations of simvastatin (0.2−0.4 μg/mL) can lead to a shift to the M2 anti-inflammatory subset in macrophages. Also, the use of N@MN-MNPS and S + N@MN-MNPS showed better outcomes than their free format low concentrations.

We also found that the effects of simvastatin on M2 macrophages at low (0.2−0.4 μg/mL) and high (0.8−2.0 μg/mL) concentrations either alone or in combination with niacin were different. At low concentrations, especially 0.2 μg/mL, both inflammatory and anti-inflammatory markers were decreased to the baseline level of expression in the M2 macrophages. The MN-MNPs induced *IL-6* in M2 populations, which is probably due to the mannose receptor-mediated cellular uptake of the NPs.[83] S@MN-MNPs (0.2 to 0.4 μg/mL) only induced *IL-6*, in doses corresponding to MN-MNPs, but the rate of *IL-6* induction is less than the free state of simvastatin, which might be due to controlled drug release of the S@MN-MNP delivery system. Both free and MN-MNP encapsulate forms of niacin, induced higher levels of *ARG1*. Whether niacin can diminish the rate of M1 polarization and thus slow atherosclerosis progression by increasing M2 macrophages in vivo is yet to be investigated.

Codelivery of simvastatin/niacin at low concentrations of simvastatin did not show any significant effect on *IL-6* expression, whereas at higher doses, induced *IL-6* expression in both short- and long-term administration occurred. However, in the case of M2 macrophages, a higher dose of simvastatin was effective in inducing *ARG1* expression. The effect of S + N@MN-MNPs showed that low concentrations of simvastatin (0.2 μg/mL) in the long term (48 h) led to a significant increase in *ARG1* expression levels versus a small increase in *IL-6*. These results showed that this concentration can be used to better deviate macrophages to M2 phenotype and stabilize their anti-inflammatory activity.

Analysis of apoptosis in treated cells showed that free simvastatin was more toxic to J774A (27.4% apoptosis) than the encapsulated form (10.3%). Interestingly, niacin induced negligible apoptosis in all forms, and the codelivery of simvastatin/niacin (S + N@MN-MNPs) modulated the induction of apoptosis, as well. Similarly, treatment of HUVECs with high levels of free simvastatin showed greater toxicity compared with encapsulated formulations, possibly due to controlled drug release. Free and encapsulated formulations of niacin and niacin/simvastatin did not induce significant cell death in HUVECs. These results are encouraging in the sense that our drug-loaded particles did not increase apoptosis in macrophages and HUVECs and were even safer than those in the free form of the drug. On the contrary to the macrophage and endothelial cell lines, treatment of murine normal liver cells with free and encapsulated simvastatin induced apoptosis, and the effect of free niacin on liver cells was even worse. However, the encapsulated formulation of simvastatin/niacin showed a lower apoptosis level in liver cells than any of the other formulations. Therefore, hepatocyte toxicity by niacin is decreased by encapsulation in mannan particles and codelivery with simvastatin.

## 5. CONCLUSIONS AND PERSPECTIVES

The results of the present study imply that the use of N@MN-MNPs might potentially prevent the progression of atherosclerosis in the early stages of the disease. Also, S + N@MN-MNPs might be effective through anti-inflammatory macrophage subset stabilization with minimum side effects on liver cells. Although simvastatin and niacin are both currently approved for treatment of patients with coronary disease with clinical and angiographically measurable benefits and lowering HDL levels, a targeted delivery approach will not only change the frequency of medication from daily to monthly or even seasonal but also ensure that the side effects


https://doi.org/10.1021/acsomega.3c06389
ACS Omega 2024, 9, 658−674

of medications prescribed on healthy tissues such as liver muscles and vascular endothelial cells will be minimized. On the other hand, due to the nature of the selected NPs, these NPs are slowly decomposed after entering the body, and the resulting iron ions are carefully removed by ferritin in the blood.[84] It is worth mentioning that the success of the present drug delivery system in the treatment of arteriosclerosis is dependent on its promising results in preclinical studies on the ApoE$^{-/-}$ mouse model, which will be considered in future works.

## ■ ASSOCIATED CONTENT

### Supporting Information

The Supporting Information is available free of charge at https://pubs.acs.org/doi/10.1021/acsomega.3c06389.

The HPLC Chromatogram, and Standard curves of Simvastatin and Niacin; the Apoptosis/Necrosis plots of cells treated with Simvastatin and Niacin, and combination treatment of Simvastatin/Niacin (PDF)

## ■ AUTHOR INFORMATION


### Corresponding Author

**Mehrnoosh Doroudchi** − *Department of Immunology, School of Medicine and Immunology Center for Excellence, School of Medicine, Shiraz University of Medical Sciences, Shiraz 71348-45794, Iran*; Email: mdoroud@sums.ac.ir, mdoroudchi@gmail.com

### Authors

**Banafsheh Rastegari** − *Diagnostic Laboratory Sciences and Technology Research Center, School of Paramedical Sciences, Shiraz University of Medical Sciences, Shiraz 71439-14693, Iran; Department of Immunology, School of Medicine, Shiraz University of Medical Sciences, Shiraz 71348-45794, Iran*; orcid.org/0000-0001-5620-2670

**Atefe Ghamar Talepoor** − *Department of Immunology, School of Medicine and Immunology Center for Excellence, School of Medicine, Shiraz University of Medical Sciences, Shiraz 71348-45794, Iran*

**Shahdad Khosropanah** − *Department of Cardiology, School of Medicine, Shiraz University of Medical Sciences, Shiraz 71348-45794, Iran*

Complete contact information is available at: https://pubs.acs.org/10.1021/acsomega.3c06389


### Notes

The authors declare no competing financial interest.

## ■ ACKNOWLEDGMENTS

This research expense was partially supported by the Shiraz University of Medical Sciences (no. 4670-01-01-1396) and also the Iran National Science Foundation to support this study (no. 98011390).

## ■ REFERENCES


(1) Song, P.; Fang, Z.; Wang, H.; Cai, Y.; Rahimi, K.; Zhu, Y.; Fowkes, F. G. R.; Fowkes, F. J.; Rudan, I. Global and regional prevalence, burden, and risk factors for carotid atherosclerosis: a systematic review, meta-analysis, and modelling study. *Lancet Global Health* **2020**, *8* (5), e721−e729.

(2) Hansson, G. K. Inflammation, atherosclerosis, and coronary artery disease. *N. Engl. J. Med.* **2005**, *352* (16), 1685−1695.

(3) Levy, D. R.; Pearson, T. A. Combination niacin and statin therapy in primary and secondary prevention of cardiovascular disease. *Clin. Cardiol.* **2005**, *28* (7), 317−320.

(4) Karimi, M.; Zare, H.; Bakhshian Nik, A.; Yazdani, N.; Hamrang, M.; Mohamed, E.; Sahandi Zangabad, P.; Moosavi Basri, S. M.; Bakhtiari, L.; Hamblin, M. R. Nanotechnology in diagnosis and treatment of coronary artery disease. *Nanomedicine* **2016**, *11* (5), 513−530.

(5) Lee, S.-G.; Oh, J.; Bong, S.-K.; Kim, J.-S.; Park, S.; Kim, S.; Park, S.; Lee, S.-H.; Jang, Y. Macrophage polarization and acceleration of atherosclerotic plaques in a swine model. *PLoS One* **2018**, *13* (3), No. e0193005.

(6) Palinski, W.; Napoli, C. Unraveling pleiotropic effects of statins on plaque rupture. *Arterioscler., Thromb., Vasc. Biol.* **2002**, *22* (11), 1745−1750.

(7) Khan, W.; Farah, S.; Domb, A. J. Drug eluting stents: developments and current status. *J. Controlled Release* **2012**, *161* (2), 703−712.

(8) Fu, H.; Alabdullah, M.; Großmann, J.; Spieler, F.; Abdosh, R.; Lutz, V.; Kalies, K.; Knöpp, K.; Rieckmann, M.; Koch, S.; et al. The differential statin effect on cytokine production of monocytes or macrophages is mediated by differential geranylgeranylation-dependent Rac1 activation. *Cell Death Dis.* **2019**, *10* (12), 880.

(9) Massonnet, B.; Normand, S.; Moschitz, R.; Delwail, A.; Favot, L.; Garcia, M.; Bourmeyster, N.; Cuisset, L.; Grateau, G.; Morel, F.; et al. Pharmacological inhibitors of the mevalonate pathway activate pro-IL-1 processing and IL-1 release by human monocytes. *Eur. Cytokine Network* **2009**, *20* (3), 112−120.

(10) Lindholm, M. W.; Nilsson, J. Simvastatin stimulates macrophage interleukin-1$\beta$ secretion through an isoprenylation-dependent mechanism. *Vasc. Pharmacol.* **2007**, *46* (2), 91−96.

(11) Loppnow, H.; Zhang, L.; Buerke, M.; Lautenschläger, M.; Chen, L.; Frister, A.; Schlitt, A.; Luther, T.; Song, N.; Hofmann, B.; et al. Statins potently reduce the cytokine-mediated *IL-6* release in SMC/MNC cocultures. *J. Cell. Mol. Med.* **2011**, *15* (4), 994−1004.

(12) Liberale, L.; Carbone, F.; Camici, G. G.; Montecucco, F. IL-1$\beta$ and statin treatment in patients with myocardial infarction and diabetic cardiomyopathy. *J. Clin. Med.* **2019**, *8* (11), 1764.

(13) Huang, B.; Jin, M.; Yan, H.; Cheng, Y.; Huang, D.; Ying, S.; Zhang, L. Simvastatin enhances oxidized-low density lipoprotein-induced macrophage autophagy and attenuates lipid aggregation. *Mol. Med. Rep.* **2015**, *11* (2), 1093−1098.

(14) Härdtner, C.; Kornemann, J.; Krebs, K.; Ehlert, C. A.; Jander, A.; Zou, J.; Starz, C.; Rauterberg, S.; Sharipova, D.; Dufner, B.; et al. Inhibition of macrophage proliferation dominates plaque regression in response to cholesterol lowering. *Basic Res. Cardiol.* **2020**, *115*, 78.

(15) Feingold, K. R.; Moser, A.; Shigenaga, J. K.; Grunfeld, C. Inflammation stimulates niacin receptor (GPR109A/HCA2) expression in adipose tissue and macrophages. *J. Lipid Res.* **2014**, *55* (12), 2501−2508.

(16) Carlson, L. A. Nicotinic acid: the broad-spectrum lipid drug. A 50th anniversary review. *J. Intern. Med.* **2005**, *258* (2), 94−114.

(17) Birjmohun, R. S.; Hutten, B. A.; Kastelein, J. J.; Stroes, E. S. Efficacy and safety of high-density lipoprotein cholesterol-increasing compounds: a meta-analysis of randomized controlled trials. *J. Am. Coll. Cardiol.* **2005**, *45* (2), 185−197.

(18) Bays, H. Safety of niacin and simvastatin combination therapy. *Am. J. Cardiol.* **2008**, *101* (8), S3−S8.

(19) Cicha, I.; Garlichs, C. D.; Alexiou, C. Cardiovascular therapy through nanotechnology-how far are we still from bedside? *Eur. J. Nanomed.* **2014**, *6* (2), 63−87.

(20) Matuszak, J.; Lutz, B.; Sekita, A.; Zaloga, J.; Alexiou, C.; Lyer, S.; Cicha, I. Drug delivery to atherosclerotic plaques using superparamagnetic iron oxide nanoparticles. *Int. J. Nanomed.* **2018**, *13*, 8443−8460.

(21) Ghanbarei, S.; Sattarahmady, N.; Zarghampoor, F.; Azarpira, N.; Hossein-Aghdaie, M. Effects of labeling human mesenchymal stem cells with superparamagnetic zinc-nickel ferrite nanoparticles on

cellular characteristics and adipogenesis/osteogenesis differentiation. *Biotechnol. Lett.* **2021**, *43* (8), 1659−1673.
(22) Mokhtarian, F.; Rastegari, B.; Zeinali, S.; Tohidi, M.; Karbalaei-Heidari, H. R. Theranostic Effect of Folic Acid Functionalized MIL-100 (Fe) for Delivery of Prodigiosin and Simultaneous Tracking-Combating Breast Cancer. *J. Nanomater.* **2022**, *2022*, 1−16.
(23) Tietze, R.; Lyer, S.; Dürr, S.; Struffert, T.; Engelhorn, T.; Schwarz, M.; Eckert, E.; Göen, T.; Vasylyev, S.; Peukert, W.; et al. Efficient drug-delivery using magnetic nanoparticles biodistribution and therapeutic effects in tumour bearing rabbits. *Nanomed. Nanotechnol. Biol. Med.* **2013**, *9* (7), 961−971.
(24) Ma, Y.-H.; Wu, S.-Y.; Wu, T.; Chang, Y.-J.; Hua, M.-Y.; Chen, J.-P. Magnetically targeted thrombolysis with recombinant tissue plasminogen activator bound to polyacrylic acid-coated nanoparticles. *Biomaterials* **2009**, *30* (19), 3343−3351.
(25) Zhang, Y.; Li, W.; Ou, L.; Wang, W.; Delyagina, E.; Lux, C.; Sorg, H.; Riehemann, K.; Steinhoff, G.; Ma, N. Targeted delivery of human VEGF gene via complexes of magnetic nanoparticle-adenoviral vectors enhanced cardiac regeneration. *PLoS One* **2012**, *7* (7), No. e39490.
(26) Vázquez-Mendoza, A.; Carrero, J. C.; Rodriguez-Sosa, M. Parasitic infections: a role for C-type lectins receptors. *BioMed Res. Int.* **2013**, *2013*, 1−11.
(27) Vu-Quang, H.; Muthiah, M.; Kim, Y.-K.; Cho, C.-S.; Namgung, R.; Kim, W. J.; Rhee, J. H.; Kang, S. H.; Jun, S. Y.; Choi, Y.-J.; et al. Carboxylic mannan-coated iron oxide nanoparticles targeted to immune cells for lymph node-specific MRI in vivo. *Carbohydr. Polym.* **2012**, *88* (2), 780−788.
(28) Vu-Quang, H.; Yoo, M.-K.; Jeong, H.-J.; Lee, H.-J.; Muthiah, M.; Rhee, J. H.; Lee, J.-H.; Cho, C.-S.; Jeong, Y. Y.; Park, I.-K. Targeted delivery of mannan-coated superparamagnetic iron oxide nanoparticles to antigen-presenting cells for magnetic resonance-based diagnosis of metastatic lymph nodes in vivo. *Acta Biomater.* **2011**, *7* (11), 3935−3945.
(29) Gai, X.; Tu, K.; Lu, Z.; Zheng, X. MRC2 expression correlates with TGF$\beta$1 and survival in hepatocellular carcinoma. *Int. J. Mol. Sci.* **2014**, *15* (9), 15011−15025.
(30) Dias, A.; Hussain, A.; Marcos, A.; Roque, A. A biotechnological perspective on the application of iron oxide magnetic colloids modified with polysaccharides. *Biotechnol. Adv.* **2011**, *29* (1), 142−155.
(31) Mosser, D. M.; Edwards, J. P. Exploring the full spectrum of macrophage activation. *Nat. Rev. Immunol.* **2008**, *8* (12), 958−969.
(32) De Paoli, F.; Staels, B.; Chinetti-Gbaguidi, G. Macrophage phenotypes and their modulation in atherosclerosis. *Circ. J.* **2014**, *78* (8), 1775−1781.
(33) De Gaetano, M.; Crean, D.; Barry, M.; Belton, O. M1-and M2-type macrophage responses are predictive of adverse outcomes in human atherosclerosis. *Front. Immunol.* **2016**, *7*, 275.
(34) Barrett, T. J. Macrophages in atherosclerosis regression. *Arterioscler., Thromb., Vasc. Biol.* **2020**, *40* (1), 20−33.
(35) Petty, A. J.; Li, A.; Wang, X.; Dai, R.; Heyman, B.; Hsu, D.; Huang, X.; Yang, Y. Hedgehog signaling promotes tumor-associated macrophage polarization to suppress intratumoral CD8+ T cell recruitment. *J. Clin. Invest.* **2019**, *129* (12), 5151−5162.
(36) Yu, S. S.; Lau, C. M.; Barham, W. J.; Onishko, H. M.; Nelson, C. E.; Li, H.; Smith, C. A.; Yull, F. E.; Duvall, C. L.; Giorgio, T. D. Macrophage-specific RNA interference targeting via "click", mannosylated polymeric micelles. *Mol. Pharmaceutics* **2013**, *10* (3), 975−987.
(37) Yi, B. G.; Park, O. K.; Jeong, M. S.; Kwon, S. H.; Jung, J. I.; Lee, S.; Ryoo, S.; Kim, S. E.; Kim, J. W.; Moon, W.-J.; et al. In vitro photodynamic effects of scavenger receptor targeted-photoactivatable nanoagents on activated macrophages. *Int. J. Biol. Macromol.* **2017**, *97*, 181−189.
(38) Lewis, D. R.; Petersen, L. K.; York, A. W.; Zablocki, K. R.; Joseph, L. B.; Kholodovych, V.; Prud'homme, R. K.; Uhrich, K. E.; Moghe, P. V. Sugar-based amphiphilic nanoparticles arrest atherosclerosis in vivo. *Proc. Natl. Acad. Sci. U.S.A.* **2015**, *112* (9), 2693−2698.
(39) Poh, S.; Putt, K. S.; Low, P. S. Folate-targeted dendrimers selectively accumulate at sites of inflammation in mouse models of ulcerative colitis and atherosclerosis. *Biomacromolecules* **2017**, *18* (10), 3082−3088.
(40) Zhao, Y.; Jiang, C.; He, J.; Guo, Q.; Lu, J.; Yang, Y.; Zhang, W.; Liu, J. Multifunctional dextran sulfate-coated reconstituted high density lipoproteins target macrophages and promote beneficial antiatherosclerotic mechanisms. *Bioconjugate Chem.* **2017**, *28* (2), 438−448.
(41) Hossaini Nasr, S.; Rashidijahanabad, Z.; Ramadan, S.; Kauffman, N.; Parameswaran, N.; Zinn, K. R.; Qian, C.; Arora, R.; Agnew, D.; Huang, X. Effective atherosclerotic plaque inflammation inhibition with targeted drug delivery by hyaluronan conjugated atorvastatin nanoparticles. *Nanoscale* **2020**, *12* (17), 9541−9556.
(42) Niu, H.; Zhang, D.; Zhang, S.; Zhang, X.; Meng, Z.; Cai, Y. Humic acid coated Fe3O4 magnetic nanoparticles as highly efficient Fenton-like catalyst for complete mineralization of sulfathiazole. *J. Hazard. Mater.* **2011**, *190* (1−3), 559−565.
(43) Bhatia, M. S.; Jadhav, S. D.; Bhatia, N. M.; Choudhari, P. B.; Ingale, K. B. Synthesis, characterization and quantification of simvastatin metabolites and impurities. *Sci. Pharm.* **2011**, *79* (3), 601−614.
(44) Shen, L.; Hillebrand, A.; Wang, D. Q.-H.; Liu, M. Isolation and primary culture of rat hepatic cells. *J. Visualized Exp.* **2012**, *64*, No. e3917.
(45) Charni-Natan, M.; Goldstein, I. Protocol for primary mouse hepatocyte isolation. *STAR Protoc.* **2020**, *1* (2), 100086.
(46) Kato, K.; Nitta, M.; Mizuno, T. Infrared spectroscopy of some mannans. *Agric. Biol. Chem.* **1973**, *37* (2), 433−435.
(47) Tuomisto, T. T.; Lumivuori, H.; Kansanen, E.; Häkkinen, S. K.; Turunen, M. P.; Van Thienen, J. V.; Horrevoets, A. J.; Levonen, A.-L.; Ylä-Herttuala, S. Simvastatin has an anti-inflammatory effect on macrophages via upregulation of an atheroprotective transcription factor, Kruppel-like factor 2. *Cardiovasc. Res.* **2008**, *78* (1), 175−184.
(48) Hillaireau, H.; Couvreur, P. Nanocarriers' entry into the cell: relevance to drug delivery. *Cell. Mol. Life Sci.* **2009**, *66* (17), 2873−2896.
(49) Unsoy, G.; Yalcin, S.; Khodadust, R.; Gunduz, G.; Gunduz, U. Synthesis optimization and characterization of chitosan-coated iron oxide nanoparticles produced for biomedical applications. *J. Nanopart. Res.* **2012**, *14* (11), 964.
(50) Chouly, C.; Pouliquen, D.; Lucet, I.; Jeune, J.; Jallet, P. Development of superparamagnetic nanoparticles for MRI: effect of particle size, charge and surface nature on biodistribution. *J. Microencapsulation* **1996**, *13* (3), 245−255.
(51) Dobrovolskaia, M. A.; Aggarwal, P.; Hall, J. B.; McNeil, S. E. Preclinical studies to understand nanoparticle interaction with the immune system and its potential effects on nanoparticle biodistribution. *Mol. Pharmaceutics* **2008**, *5* (4), 487−495.
(52) Yu, W.; Liu, R.; Zhou, Y.; Gao, H. Size-tunable strategies for a tumor targeted drug delivery system. *ACS Cent. Sci.* **2020**, *6* (2), 100−116.
(53) Dong, Q.; Hurst, D. R.; Weinmann, H. J.; Chenevert, T. L.; Londy, F. J.; Prince, M. R. Magnetic resonance angiography with gadomer-17: an animal study. *Invest. Radiol.* **1998**, *33* (9), 699−708.
(54) Sato, N.; Kobayashi, H.; Hiraga, A.; Saga, T.; Togashi, K.; Konishi, J.; Brechbiel, M. W. Pharmacokinetics and enhancement patterns of macromolecular MR contrast agents with various sizes of polyamidoamine dendrimer cores. *Magn. Reson. Med.* **2001**, *46* (6), 1169−1173.
(55) Moghimi, S. M.; Hunter, A. C.; Murray, J. C. Nanomedicine: current status and future prospects. *FASEB J.* **2005**, *19* (3), 311−330.
(56) Gupta, A. S. Nanomedicine approaches in vascular disease: a review. *Nanomed. Nanotechnol. Biol. Med.* **2011**, *7* (6), 763−779.
(57) Soo Choi, H.; Liu, W.; Misra, P.; Tanaka, E.; Zimmer, J. P.; Itty Ipe, B.; Bawendi, M. G.; Frangioni, J. V. Renal clearance of quantum dots. *Nat. Biotechnol.* **2007**, *25* (10), 1165−1170.


https://doi.org/10.1021/acsomega.3c06389
*ACS Omega* 2024, 9, 658−674

(58) Liu, D.; Mori, A.; Huang, L. Role of liposome size and RES blockade in controlling biodistribution and tumor uptake of GM1-containing liposomes. *Biochim. Biophys. Acta, Biomembr.* **1992**, *1104* (1), 95−101.
(59) Barua, S.; Mitragotri, S. Challenges associated with penetration of nanoparticles across cell and tissue barriers: a review of current status and future prospects. *Nano today* **2014**, *9* (2), 223−243.
(60) Li, B.; Jia, D.; Zhou, Y.; Hu, Q.; Cai, W. In situ hybridization to chitosan/magnetite nanocomposite induced by the magnetic field. *J. Magn. Magn. Mater.* **2006**, *306* (2), 223−227.
(61) Arora, W. Superparamagnetic iron oxide nanoparticles: magnetic nanoplatforms as drug carriers. *Int. J. Nanomed.* **2012**, *7*, 3445.
(62) Gregorio-Jauregui, K. M.; Pineda, M.; Rivera-Salinas, J. E.; Hurtado, G.; Saade, H.; Martinez, J. L.; Ilyina, A.; López, R. G. One-step method for preparation of magnetic nanoparticles coated with chitosan. *J. Nanomater.* **2012**, *2012*, 1−8.
(63) Williamson, N. R.; Fineran, P. C.; Leeper, F. J.; Salmond, G. P. The biosynthesis and regulation of bacterial prodiginines. *Nat. Rev. Microbiol.* **2006**, *4* (12), 887−899.
(64) Fang, C.; Xiong, Z.; Qin, H.; Huang, G.; Liu, J.; Ye, M.; Feng, S.; Zou, H. One-pot synthesis of magnetic colloidal nanocrystal clusters coated with chitosan for selective enrichment of glycopeptides. *Anal. Chim. Acta* **2014**, *841*, 99−105.
(65) Lee, J.-Y.; Chung, S.-J.; Cho, H.-J.; Kim, D.-D. Bile acid-conjugated chondroitin sulfate A-based nanoparticles for tumor-targeted anticancer drug delivery. *Eur. J. Pharm. Biopharm.* **2015**, *94*, 532−541.
(66) Anirudhan, T. S.; Divya, P. L.; Nima, J. Synthesis and characterization of novel drug delivery system using modified chitosan based hydrogel grafted with cyclodextrin. *Chem. Eng. J.* **2016**, *284*, 1259−1269.
(67) Schleich, N.; Sibret, P.; Danhier, P.; Ucakar, B.; Laurent, S.; Muller, R. N.; Jérôme, C.; Gallez, B.; Préat, V.; Danhier, F. Dual anticancer drug/superparamagnetic iron oxide-loaded PLGA-based nanoparticles for cancer therapy and magnetic resonance imaging. *Int. J. Pharm.* **2013**, *447* (1−2), 94−101.
(68) Mirzaeinia, S.; Zeinali, S.; Budisa, N.; Karbalaei-Heidari, H. R. Targeted Codelivery of Prodigiosin and Simvastatin Using Smart BioMOF: Functionalization by Recombinant Anti-VEGFR1 scFv. *Front. bioeng. biotechnol.* **2022**, *10*, 866275.
(69) Lin, L.; Xu, W.; Liang, H.; He, L.; Liu, S.; Li, Y.; Li, B.; Chen, Y. Construction of pH-sensitive lysozyme/pectin nanogel for tumor methotrexate delivery. *Colloids Surf., B* **2015**, *126*, 459−466.
(70) Unsoy, G.; Khodadust, R.; Yalcin, S.; Mutlu, P.; Gunduz, U. Synthesis of Doxorubicin loaded magnetic chitosan nanoparticles for pH responsive targeted drug delivery. *Eur. J. Pharm. Sci.* **2014**, *62*, 243−250.
(71) Rastegari, B.; Karbalaei-Heidari, H. R.; Zeinali, S.; Sheardown, H. The enzyme-sensitive release of prodigiosin grafted $\beta$-cyclodextrin and chitosan magnetic nanoparticles as an anticancer drug delivery system: Synthesis, characterization and cytotoxicity studies. *Colloids Surf., B* **2017**, *158*, 589−601.
(72) Chen, X.; Yao, X.; Wang, C.; Chen, L.; Chen, X. Mesoporous silica nanoparticles capped with fluorescence-conjugated cyclodextrin for pH-activated controlled drug delivery and imaging. *Microporous Mesoporous Mater.* **2015**, *217*, 46−53.
(73) Wang, C.; Huang, L.; Song, S.; Saif, B.; Zhou, Y.; Dong, C.; Shuang, S. Targeted delivery and pH-responsive release of stereo-isomeric anti-cancer drugs using $\beta$-cyclodextrin assemblied Fe3O4 nanoparticles. *Appl. Surf. Sci.* **2015**, *357*, 2077−2086.
(74) Shahbazi, M.-A.; Sedighi, M.; Bauleth-Ramos, T. s.; Kant, K.; Correia, A.; Poursina, N.; Sarmento, B.; Hirvonen, J.; Santos, H. A. Targeted reinforcement of macrophage reprogramming toward M2 polarization by IL-4-loaded hyaluronic acid particles. *ACS Omega* **2018**, *3* (12), 18444−18455.
(75) Li, Q.-z.; Sun, J.; Han, J.-j.; Qian, Z.-j. Anti-inflammation of simvastatin by polarization of murine macrophages from M1 phenotype to M2 phenotype. *Zhonghua Yi Xue Za Zhi* **2013**, *93* (26), 2071−2074.
(76) Montserrat-de la Paz, S.; Naranjo, M. C.; Lopez, S.; Abia, R.; Muriana, F. J. G.; Bermudez, B. Niacin and its metabolites as master regulators of macrophage activation. *J. Nutr. Biochem.* **2017**, *39*, 40−47.
(77) Montserrat-de la Paz, S.; Naranjo, M. C.; Lopez, S.; Abia, R.; Muriana, F. J.; Bermudez, B. Niacin and olive oil promote skewing to the M2 phenotype in bone marrow-derived macrophages of mice with metabolic syndrome. *Food Funct.* **2016**, *7* (5), 2233−2238.
(78) Ganapathy, V.; Thangaraju, M.; Prasad, P. D.; Martin, P. M.; Singh, N. Transporters and receptors for short-chain fatty acids as the molecular link between colonic bacteria and the host. *Curr. Opin. Pharmacol.* **2013**, *13* (6), 869−874.
(79) Wakade, C.; Giri, B.; Malik, A.; Khodadadi, H.; Morgan, J. C.; Chong, R. K.; Baban, B. Niacin modulates macrophage polarization in Parkinson's disease. *J. Neuroimmunol.* **2018**, *320*, 76−79.
(80) Salem, H. A.; Wadie, W. Effect of niacin on inflammation and angiogenesis in a murine model of ulcerative colitis. *Sci. Rep.* **2017**, *7* (1), 7139.
(81) Singh, N.; Gurav, A.; Sivaprakasam, S.; Brady, E.; Padia, R.; Shi, H.; Thangaraju, M.; Prasad, P. D.; Manicassamy, S.; Munn, D. H.; et al. Activation of Gpr109a, receptor for niacin and the commensal metabolite butyrate, suppresses colonic inflammation and carcinogenesis. *Immunity* **2014**, *40* (1), 128−139.
(82) Moehle, M. S.; West, A. B. M1 and M2 immune activation in Parkinson's disease: foe and ally? *Neuroscience* **2015**, *302*, 59−73.
(83) Tanaka, T.; Narazaki, M.; Kishimoto, T. *IL-6* in inflammation, immunity, and disease. *Cold Spring Harbor Perspect. Biol.* **2014**, *6* (10), a016295.
(84) Volatron, J.; Carn, F.; Kolosnjaj-Tabi, J.; Javed, Y.; Vuong, Q. L.; Gossuin, Y.; Ménager, C.; Luciani, N.; Charron, G.; Hémadi, M.; et al. Ferritin protein regulates the degradation of iron oxide nanoparticles. *Small* **2017**, *13* (2), 1602030.


https://doi.org/10.1021/acsomega.3c06389
*ACS Omega* 2024, 9, 658−674